Mathematics and Computers in Simulation 228 (2025) 178–201

Contents lists available at ScienceDirect

Mathematics and Computers in Simulation

journal homepage: www.elsevier.com/locate/matcom

Original articles

Inner loop model predictive control and outer loop PI reference governor for PMSMs with input and state saturation for torque control

Tanja Zwerger [a], Paolo Mercorelli [b,*]

[a] Rolls Royce Power Systems GmbH, Maybachplatz 1, Friedrichshafen, 88045, Germany
[b] Leuphana University of Lueneburg, Universitaetsallee 1, Lueneburg, 21335, Germany

ARTICLE INFO

Keywords:
PMSM
PI-MPC
Decoupled system
Saturation
EKF

ABSTRACT

This contribution considers a torque control scheme consisting of model predictive control (MPC) in the inner control loop together with PI reference governor in the outer control loop and a decoupling feedforward control for an isotropic permanent magnet synchronous machine (PMSM). This innovative approach is known in literature as PI-MPC dual loop control. A particular emphasis is given to the control governor strategy which is the outer loop PI reference governor and allows to regulate the machine in the flux weakening region and is therefore only active for field weakening. In this context the analysis of the stability based on Lyapunov' approach of the control loop in flux weakening region is shown. The desired currents represent the reference currents for the MPC, which forms the inner control loop. The MPC is adapted using an extended Kalman filter (EKF), which estimates inductance of the electrical system in dq coordinates by using a bivariate polynomial. Compared measurements with a hardware-in-the-loop (HIL) system show the effectiveness of the proposed control scheme with respect to a standard PI controller in inner loop (PI-PI scheme) in the presence of saturated inputs and state of a PMSM. The proposed MPC uses just an optimal, proportional control and thus avoids windup effects. Measurement results in the presence of input and state saturations show that MPC is working without overshoot in the currents which leads to less needed power in input.

1. Introduction

Permanent Magnet Synchronous Machines (PMSMs) have become increasingly important in recent years, partly due to the growing influence of electromobility in the private transport and off-highway markets. The optimization of the power density resulted in the preference of PMSMs. PMSMs benefit from the improvement in magnetic materials like neodymium iron boron magnets [1]. One of the most important tasks in PMSMs which are used for traction, is represented by the general problem of the torque control in different working regions of the motor, see [2], and more recently in [3]. In the last years these machines found applications in many industrial fields but in particular in automotive applications for traction- and as servomotors. The control of these machines is one of the most important and decisive issues to guarantee their use in an optimal way in terms of energy consumption, functionality and long life. One of the emerging control strategies is model predictive control (MPC), a widely used control technology for these purposes. The use of the MPC in combination with a PMSM has already been described frequently.

* Corresponding author.
E-mail address: paolo.mercorelli@leuphana.de (P. Mercorelli).

https://doi.org/10.1016/j.matcom.2024.08.006
Received 21 January 2024; Received in revised form 9 May 2024; Accepted 7 August 2024
Available online 31 August 2024
0378-4754/© 2024 The Author(s). Published by Elsevier B.V. on behalf of International Association for Mathematics and Computers in Simulation (IMACS). This is an open access article under the CC BY-NC-ND license (http://creativecommons.org/licenses/by-nc-nd/4.0/).

For example, in [4], a continuous control set MPC is presented, that shows clear advantages regarding torque ripples and total harmonic distortion (THD). In [5], the robustness of the MPC is improved by proposing a compensated scheme with simplified repetitive control (SRC). Another example for the use of an MPC in a PMSM control application is given in [6], where an optimized finite control set MPC strategy based on disturbance feedback rejection control for PMSMs is presented. The MPC is also often used to control the PMSM in the saturation region, taking current and voltage limits into account, see [7]. In terms of torque control, to improve the performance of motor controllers, an MPC method is employed for high-speed and in-wheel motor drives in [8]. In another context also [9] implements an MPC for duty cycle optimization. To round off this excerpt of possible applications of the MPC for PMSM control, the article in [10] should be mentioned here, too, where a nonlinear MPC for PMSM torque control shows the benefits of MPC for high performance applications. In the following paper, a method of MPC is presented which, due to decoupling, allows the computational effort to be significantly reduced. The problem of conventional MPC is the susceptibility to parameter variations and thus the strong dependence on the accuracy of the system model. In the presented method, these drawbacks are overcome by using an extended Kalman filter (EKF), which gives the estimated quantities to the decoupling equations of the MPC. The MPC therefore operates in an inner control loop. When the motor is working in the constant power region, a PI reference governor is added to the control scheme in an outer control loop and guarantees accuracy in the steady state. The resulting control method is a PI-MPC, which offers significant advantages particularly in the area of field weakening, which often tends to be less stable. The contribution of this paper can be summarized in the following items, for the general problem of torque control in different working regions of the PMSM:

- a saturation in the inductance which is generated by higher currents together with an input voltage saturation
- an EKF is used to estimate the inductance of the PMSM to adjust the feedforward control and realize a decoupled system controlled by a proposed model predictive control (MPC) system in an inner control loop and a PI reference governor in an outer control loop, resulting in a PI-MPC control strategy, that is mainly active during field weakening in constant power region
- due to saturation behavior of the inductances, the estimation of these by the EKF becomes even more important, as this can guarantee a sufficiently good adaptive decoupled model for the MPC in order to obtain a convex optimization problem
- an MPC is carried out for constant torque and for constant power region
- a proof of a theorem concerning the stability of the proposed control scheme for the constant power region. The stability analysis is done for PI-MPC given with the help of more general results for the MPC in the form of two propositions in the Appendix, as [11] already shows an analysis for PI-PI
- soft switching between constant torque and constant power region is handled by a Sigmoid function that guarantees a smooth transition between the two regions
- measured validated results in an industrial project conducted by Rolls-Royce Power Systems using hardware-in-the-loop (HIL) are presented. The results in terms of torque control of the proposed MPC are compared with a control structure consisting of an inner and outer proportional-integral (PI-PI) controller.

1.1. MPC as anti-saturating control structure

Anti-saturating structures are important in control to avoid windup, in the presence of integral action, and more in general to avoid reduction of dynamic performances of the controlled system. To apply model based prediction strategies to avoid or to reduce the effect of saturation is a common used technique with some variations, see [12]. In [13] and in [14] an improved anti-integral saturation mechanism is suggested in which a predictive functional control method is incorporated. In [15] an improvement of MPC, predictive functional control has the advantage to handle uncertainties and system delays with reduced computation. The tests and measurements, described in the following text, were carried out with an isotropic machine, where the inductance is approximately the same for L_d and L_q. Since the machine equations of the anisotropic machine are also valid for the isotropic machine, the equations of the anisotropic machine will be used in the further course for the sake of completeness. The control of the isotropic machine changes in comparison to the anisotropic machine, since a pure quadrature current i_q is inserted below the rated speed during constant torque region and no maximum torque per ampere (MTPA) control is applied. MPC is a type of feedback control that uses online process optimization. It uses a decoupling strategy to realize the simple algorithm to be applied.

In order to realize decoupling, the system must identify the parameters of the motor. In this sense the performances of the Kalman filter (KF) are important to accurately identify these parameters even though in the presence of uncertainties and disturbances. In particular, in the presence of saturation the inductances change over time. Moreover, the importance of the KF is also in the context of the adaptive MPC. In fact, the MPC implemented here does not contain an integral action and is therefore structurally windup-free, and its linear model structure preserves optimality. These advantages are particularly useful in the area of field weakening, where the PI-MPC control strategy is clearly demonstrated by the Sigmoid function. However, the application of this MPC structure requires the estimation of the parameters to be predicted using a linear, albeit time-varying, system. In fact, the nonlinearity, due to the saturation effect is canceled by the decoupling action which should be adapted through an online identification to guarantee the cancellation. While maintaining linearity, a convex optimization problem is preserved in the structure of the proposed MPC, and a unique off-line solution of this optimization problem can be computed. The advantage of this procedure consists of a reduction of the calculation load. The proposed control scheme is shown in Fig. 1.

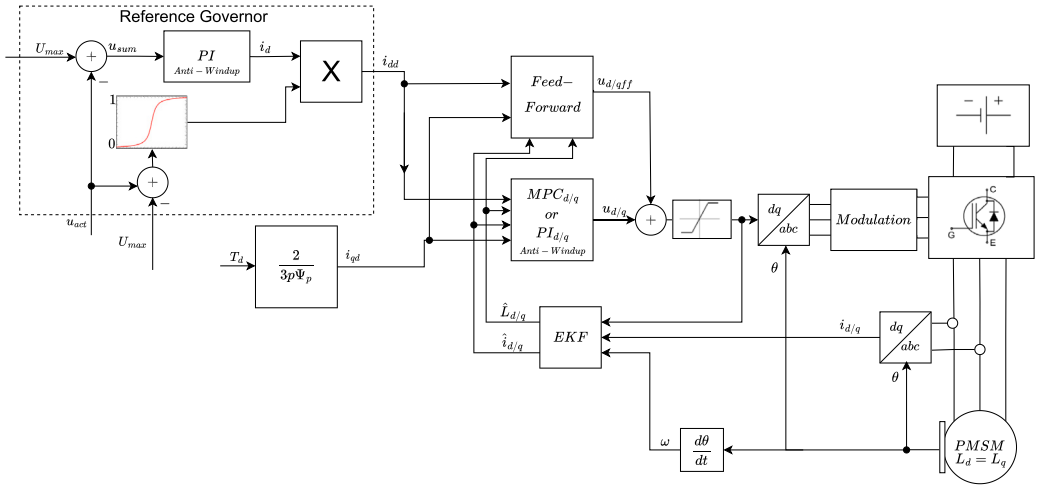

Fig. 1. Simulation setup including MPC or PI control with a PI reference governor for i_{dd}.

1.2. PI-MPC for constant torque and constant power region

The vector control of a controlled PMSM is usually divided into two ranges. While the constant torque region is controlled at the current control limit, the field weakening or constant power region is controlled at the voltage limit. For PMSM with reluctance torque, this results in the control rules of maximum torque per ampere (MTPA) and maximum torque per voltage (MTPV). For an isotropic machine, on the other hand, the associated quadrature current i_q is usually calculated from the electromagnetic main torque T. As soon as the constant power region is entered by reaching the maximum permissible voltage limit, an additional negative direct current i_d is induced in order to be able to further increase the speed ω. MPC is a new trend to control PMSM in saturation condition, see [16]. In this paper, a PMSM is controlled by an MPC structure in an inner control loop with a PI reference governor in an outer control loop, which is responsible for the i_d setpoint value of the MPC by specifying $i_d < 0$ in the flux weakening range. The results are compared with a PI controller using in the same way a PI reference governor which is responsible to regulate the flux weakening condition. Just the MPC structure is considered in the analysis of the stability. Indeed, in the literature, such as [11], the stability of a control scheme using a PI current controller based on passivity is studied. For the MPC the details for stability analysis will be discussed in Section 6. As shown in [17], for example, the combination of MPC in inner loop with PI control in outer loop can help to reduce the value of the total harmonic distortion (THD) of the tracking current. In [18] it is also shown that the combination of PI and MPC control structure, with MPC in outer loop, has a significantly higher degree of robustness. In the proposed approach, the roles of the two controller are inverted and a PI-MPC control strategy, which is active in the field weakening range is proposed. The PI-MPC strategy is applied in the field weakening range that is more critical to control, i.e. the constant power range, combines the advantages of the MPC, which avoids overshooting due to the proportional behavior, with those of the PI controller, which is able to demonstrate stationary accuracy. The resulting control behavior is therefore more robust, which is an enormous advantage in the field weakening range. The new trend in PI-MPC can been seen in [19] and in [20]. In particular, in the latest work, the PI voltage controller is required to achieve the adjustable voltage control and to produce the input current reference to the predictive algorithm. The inner loop MPC, thanks to its optimal nature, reduces the input current ripple.

1.3. EKF to estimate the inductance of the PMSM

Modern control methods for three-phase machines have been intensively researched in recent years in order to make even better use of the expensive and power-dense PMSM machines. An effort was put into the development of processes that work, as pointed out, using MPC. To implement an MPC, many different variants of observers were developed to implement this kind of control. Observers are algorithm structures that allow to realize virtual sensors to estimate states and parameters indirectly through the measurements of a suitable reduced number of states of the system. EKFs can be used as observer for the estimation and they are widely used in this context which is generically called sensorless control. Sensorless control is the name of modern stream in academic research and in any kind of industrial applications in which a minimal number of sensors is involved to monitor and to control systems with the help of observers (for example, see [21]) and in particular for electrical machines [22]. As explained, the modern control techniques for electrical motors are model-based ones and are often combined with sensorless control strategies to reduce the number of sensors; as seen in [23,24] and more recently in [25] and in [26]. Sensorless control is one of the problems most examined with different approaches. In [27], and very recently in [28–30], different observers for the sensorless control of PMSMs with online resistance and inductance estimation are proposed. For the EKF, which is often used for PMSM and for all Kalman filters, the tuning of covariance matrices remains the crucial issue, see [31,32]. After the pioneering work of Kalman, see [33], a continuous development of concepts for the tuning of EKFs was proposed. Apart from manual tuning by trial and error, which is still

widely used, many other tuning solutions have been proposed over the years. One of the first contributions in this context, but still one of the most widely used, was proposed in the 1970s by [34]. In this paper, statistics are generated based on the noise sample produced by the filter itself, which is determined as the difference between the estimated and measured quantities. In the context of motor drives, an extensive data set obtained from a sensor-controlled drive was used in [35] to optimize the tuning of the EKF matrices using a generic algorithm. Another alternative method is proposed in [36]. The paper considers the ratio between $\mathbf{Q}$ and $\mathbf{R}_w$ instead of their individual values to calculate the Kalman gain at each step of the algorithm. In the belief that automation of the tuning process is the key to wider application of EKF in frequency converters, a master–slave (MS) structure has recently been proposed in the literature as a further step. This structure is designed for online determination and tracking of the noise covariance matrix. The concept of the MS algorithm was originally introduced as an extension of the unscented Kalman filter (UKF), see [37]. Later, a simplified version of the algorithm was proposed in [38–40], which uses a linear Kalman filter (KF) as a secondary (side) filter. Nevertheless, the problem of tuning an EKF still remains an open problem related to the application of EKF. More specifically, for PMSM, we can consider two important approaches that are frequently used in applications with anisotropic machines: MTPA and maximum torque per voltage (MTPV) strategy. MTPA control strategy is employed to obtain the maximal torque per ampere. To estimate the state of a system, an EKF is often used. In the field of synchronous machines, different contributions appeared recently, e.g. [41,42], in which a comparison between EKFs and sliding mode observers is proposed in the presence of measurement noise. Recently, through a sensitivity analysis, the contributions [43,44] investigated the influence of model uncertainty on the observed position and the robustness of a proportional integral observer in current control of PMSM drives. Also interesting is the paper in [45], where an infinite amount of mechanical inertia of the drive is considered to simplify the KF structure with results of a constant velocity. In [46] variants of EKF are used to estimate the currents $i_{\alpha,\beta}$ in the stationary α, β reference frame, together with the mechanical rotor velocity and the electrical rotor angle.

The main nomenclature

u_d: direct voltage input
u_q: quadrature voltage input
i_d: direct current
i_q: quadrature current
i_{dd}: desired direct current
i_{qd}: desired quadrature current
ω_r: mechanical machine speed
ω: electrical machine speed, $\omega = p\omega_r$
p: couple of magnetic poles
R_s: coil resistance
L_d: direct inductance
L_q: quadrature inductance
Ψ_p: permanent magnet flux
T: electromagnetic torque
T_d: desired torque
T_l: load torque
ψ_d: direct flux component
ψ_q: quadrature flux component
θ: electrical angle of the rotor
θ_d: coefficient polynomial for calculation of L_d
θ_q: coefficient polynomial for calculation of L_q
u_{act}: actual system voltage
U_{nom}: nominal DC link voltage

1.4. Main contribution and structure of the paper

The main contribution of this paper is in the context of the general problem of torque control in different control regions of the PMSM. This paper shows, once the system is decoupled, how a decoupled MPC can be applied in combination with an EKF in a very simple way to minimize input and state saturating effect for a system in the presence of bounded inputs. A control scheme, as represented in Fig. 1, is proposed to control a PMSM. The paper is organized in the following way: Section 2 considers the description of the physical systems; Section 3 gives an overview on the whole control strategy. Section 4 shows the structure of the proposed EKF. Section 5 shows how the system is decoupled and how MPC, together with the EKF, is implemented to realize the prediction and to adapt the PI reference governor. Moreover in Section 5 the proof of a proposition which states the asymptotic stability of the proposed scheme is shown with the help of two propositions reported in the Appendix. Measurement results taken with Typhoon HIL402 and a comparison between PI-MPC and PI-PI controller are discussed in Section 7. The conclusion closes the paper.

2. Description of the physical systems

One of the most frequently used models in PMSM control for the implementation of field-oriented control is the machine model transformed into dq coordinates, which corresponds to a rotorfixed PMSM machine model. The direct quantities d and q resulting

from the so-called Clarke–Park transformation can now be controlled much more easily, as shown in [47] or [48], for example. As to see in (7), i_d, i_q, u_d and u_q are the dq-components of the stator currents and voltages in synchronously rotating rotor reference frame; ω is the rotor electrical angular speed; the parameter R_s is the stator resistance, L_d and L_q are the d-axis and q-axis inductances, Ψ_p is the magnetic flux and p is the number of couples of permanent magnets, respectively. If the following model is considered:

$$u_d(t) = i_d(t)R_s + \frac{d\psi_d(t)}{dt} - \omega(t)\psi_q(t), \tag{1}$$

$$u_q(t) = i_q(t)R_s + \frac{d\psi_q(t)}{dt} + \omega(t)\psi_d(t), \tag{2}$$

with

$$\psi_d(t) = L_d(t)i_d(t) + \Psi_p \tag{3}$$

and

$$\psi_q(t) = L_q(t)i_q(t). \tag{4}$$

That leads to the following relation:

$$\frac{di_d(t)}{dt} = \frac{u_d(t)}{L_d(t)} - \frac{i_d(t)R_s}{L_d(t)} + \frac{\omega(t)L_q(t)i_q(t)}{L_d(t)} \tag{5}$$

and

$$\frac{di_q(t)}{dt} = \frac{u_q(t)}{L_q(t)} - \frac{i_q(t)R_s}{L_q(t)} - \frac{\omega(t)L_d(t)i_d(t)}{L_q(t)} - \frac{\omega(t)\Psi_p}{L_q(t)}. \tag{6}$$

The electrical system in dq-coordinates can then be represented as follows:

$$\begin{bmatrix} \frac{di_d(t)}{dt} \\ \frac{di_q(t)}{dt} \end{bmatrix} = \begin{bmatrix} \frac{-R_s}{L_d(t)} & \omega(t)\frac{L_q(t)}{L_d(t)} \\ -\omega(t)\frac{L_d(t)}{L_q(t)} & \frac{-R_s}{L_q(t)} \end{bmatrix} \begin{bmatrix} i_d(t) \\ i_q(t) \end{bmatrix} + \begin{bmatrix} \frac{1}{L_d(t)} & 0 \\ 0 & \frac{1}{L_q(t)} \end{bmatrix} \begin{bmatrix} u_d(t) \\ u_q(t) \end{bmatrix} - \begin{bmatrix} 0 \\ \frac{\Psi_p\omega(t)}{L_q(t)} \end{bmatrix}. \tag{7}$$

The electromagnetic torque can be expressed with:

$$T(t) = \frac{3}{2}p\left\{ i_q(t)\Psi_p + (L_d(t) - L_q(t))i_d(t)i_q(t) \right\}. \tag{8}$$

3. MPC control structure with PI reference governor

In Fig. 1 an MPC as well as a PI control for constant torque and constant power region is presented. The reference governor is active after soft switching to the constant power region and is implemented as additive PI controller. The PI-MPC control strategy, which is active mainly in the field weakening range that is more critical to control, also known as the constant power range, combines the advantages of the MPC, which avoids overshooting due to the proportional behavior, with those of the PI controller, which is able to demonstrate stationary accuracy. The resulting control behavior is therefore more robust, which is an enormous advantage especially in the field weakening range. Soft switching from constant torque to constant power region must not be done harshly, otherwise the voltages and currents in the DC link of the inverter may oscillate, which could result in damage to the component. Therefore, a soft switching of the two regions by means of a Sigmoid function is presented here, the ramp of which is adjustable. For the constant torque region, the calculation for i_d goes towards 0. Only when the voltage reaches the voltage limit with U_{max} (considering a certain tolerance of approx. 5%–8%), the control of i_{dd} by reference governor becomes effective and a negative current i_d is impressed into the further control loop.

3.1. Sigmoid function for soft switching from constant torque to constant power region

Considering a Sigmoid function which is based on an arctan-function with adjustable limits and a shift up to zero, see Fig. 2, then

$$i_{dd}(t) = \frac{1}{\pi}\arctan((u_{act}(t) - U_{max})\gamma)i_d(t) + \frac{1}{2}i_d(t). \tag{9}$$

The arctan function usually converges very slow. For higher values for γ it gets close to its final values and the speed is adjustable. With a calculation like in (9) the values in the limits are similar to a logistic function with 0 at $-\infty$ and 1 at ∞. The inputs of the Sigmoid function are the maximum voltage, which is defined with:

$$U_{max} = \frac{U_{nom}}{\sqrt{3}}0.95, \tag{10}$$

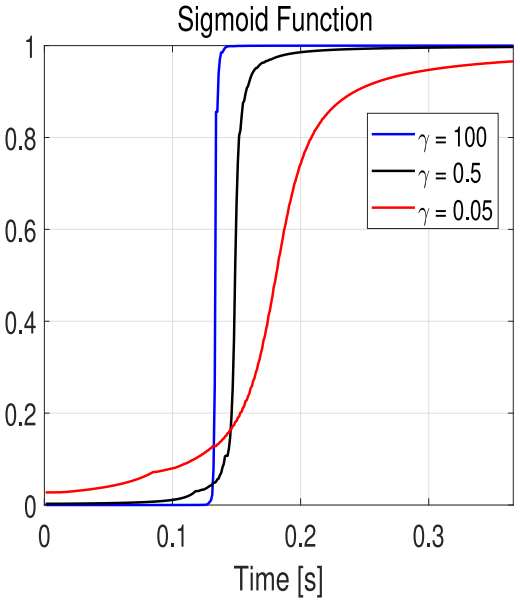

Fig. 2. Course of Sigmoid function for different values of γ.

wherein the nominal voltage U_{nom} is defined as the DC link voltage which is given by a stabilized voltage source with a HV battery. HV here stands for the abbreviation high voltage in the automotive sector and denotes a voltage of 60 V to 1500 V in each case DC. The amount of the nominal DC link voltage U_{nom} in the considered system is 400 V. The actual system voltage then is calculated with

$$u_{act}(t) = \sqrt{u_d^2(t) + u_q^2(t)} \tag{11}$$

or

$$u_{act}(t) = \omega(t)\sqrt{(L_q(t)i_q(t))^2 + (L_d(t)i_d(t) + \Psi_p)^2}. \tag{12}$$

An overview over the course of the Sigmoid function for different values of γ is given in Fig. 2.

4. EKF for parameter estimation

The Kalman filter is one of the most important methods for determining non-measurable system variables and uses the mathematical equations presented below for this purpose. These serve the minimization of the mean value of the quadratic error and estimate past as well as future states. The equations can be divided into two types, the time update or 'prediction' equations, with:

$$\hat{\mathbf{x}}^-(k+1) = \mathbf{f}(\hat{\mathbf{x}}(k), \mathbf{u}(k), \mathbf{w}(k)), \quad k \in \mathbb{N} \tag{13}$$

and

$$\mathbf{P}^-(k+1) = \mathbf{J}(k+1)\mathbf{P}(k)\mathbf{J}(k+1)^T + \mathbf{Q}, \tag{14}$$

and the measurement update or 'correction' equations with:

$$\mathbf{K}(k+1) = \mathbf{P}^-(k+1)\mathbf{H}^T(\mathbf{H}\mathbf{P}^-(k+1)\mathbf{H}^T + \mathbf{R}_w)^{-1}, \tag{15}$$

$$\hat{\mathbf{x}}(k+1) = \hat{\mathbf{x}}^-(k+1) + \mathbf{K}(k+1)(\mathbf{z}(k+1) - \mathbf{H}\hat{\mathbf{x}}^-(k+1)), \tag{16}$$

and

$$\mathbf{P}(k+1) = (\mathbf{I} - \mathbf{K}(k+1)\mathbf{H})\mathbf{P}^-(k+1). \tag{17}$$

The time update process uses Eq. (13) to project the state, in which function $\mathbf{f}(\hat{\mathbf{x}}, \mathbf{u}, \mathbf{w})$ represents a nonlinear field used to model the considered system. Eq. (14) is the a priori estimate error covariance with the calculated Jacobian matrix $\mathbf{J}$. In the measurement update process, the first step is to calculate the Kalman gain in (15). Eq. (16) gives the a posteriori state estimation and the last step is to calculate the a posteriori estimation of the error covariance in (17). A very good clear summary is given by [49].

4.1. EKF structure to estimate inductance

In [50], it was shown that by using a feedforward action it is possible to obtain a decoupling of the electrical dynamics. This is realized in [50] using an adaptive feedforward control with a KF, as shown in Fig. 1. To get a better model for the EKF, at first a bivariate polynomial has to be calculated. The coefficients were determined by measuring 9 points of the PMSM. This underlines the added value of the EKF, which is able to estimate the missing areas and thus makes a highly granular measurement unnecessary. The advantages are that the often time-consuming PMSM measurement is no longer necessary, which is not or only incompletely possible even with an already installed machine. As shown in [51], the equations for the calculated bivariate polynomials for the inductances are calculated as

$$L_d(t) = \Theta_d(1) i_d(t) i_q(t) + \Theta_d(2) i_d(t) + \Theta_d(3) i_q(t) + \Theta_d(4). \tag{18}$$

and

$$L_q(t) = \Theta_q(1) i_d(t) i_q(t) + \Theta_q(2) i_q(t) + \Theta_q(3) i_d(t) + \Theta_q(4). \tag{19}$$

with $\Theta_d(1)$, $\Theta_d(2)$, …, $\Theta_d(4)$ and $\Theta_q(1)$, $\Theta_q(2)$, …, $\Theta_q(4)$ as the single elements of the calculated vectors Θ_d and Θ_q. The inductances L_d and L_q are calculated in dependence for its currents and they are calculated offline in a static least squares procedure as in [51]. The combined EKF is realized using estimated values of ω, L_d and L_q to adapt the feedforward action of the control system. [51] gives a good overview for the calculation of the bivariate polynomial and the consideration in an EKF for estimation of the states L_d and L_q. The equations for the bivariate polynomial expressed by [51] are utilized as a model of $L_{d/q}$ in the equations of the EKF. The equations for the combined EKF then are as follows:

$$\tilde{i_d}(k) = \frac{i_d(k+1) - i_d(k)}{Ts} = \frac{u_d(k)}{L_d(k)} - \frac{i_d(k) R_s}{L_d(k)} + \frac{\omega(k) L_q(k) i_q(k)}{L_d(k)}. \tag{20}$$

$$\tilde{i_q}(k) = \frac{i_q(k+1) - i_q(k)}{Ts} = \frac{u_q(k)}{L_q(k)} - \frac{i_q(k) R_s}{L_q(k)} - \frac{\omega(k) L_d(k) i_d(k)}{L_q(k)} - \frac{\omega(k) \Psi_p}{L_q(k)}. \tag{21}$$

For the calculated inductance L_d and L_q in (18) and (19), the discretization by forward Euler is as follows:

$$\begin{aligned} \frac{L_d(k+1) - L_d(k)}{Ts} &= \Theta_d(1) i_q(k) \tilde{i_d}(k) + \Theta_d(1) i_d(k) \tilde{i_q}(k) \\ &\quad + \Theta_d(2) \tilde{i_d}(k) + \Theta_d(3) \tilde{i_q}(k). \end{aligned} \tag{22}$$

$$\begin{aligned} \frac{L_q(k+1) - L_q(k)}{Ts} &= \Theta_q(1) i_q(k) \tilde{i_d}(k) + \Theta_q(1) i_d(k) \tilde{i_q}(k) \\ &\quad + \Theta_q(2) \tilde{i_d}(k) + \Theta_q(3) \tilde{i_q}(k). \end{aligned} \tag{23}$$

$$\begin{bmatrix} \hat{i}_d^-(k+1) \\ \hat{i}_q^-(k+1) \\ \hat{L}_d^-(k+1) \\ \hat{L}_q^-(k+1) \end{bmatrix} = \begin{bmatrix} \hat{i}_d(k) - \frac{T_s R_s \hat{i}_d(k)}{\hat{L}_d(k)} + \frac{T_s p \omega_r(k) \hat{i}_q(k) \hat{L}_q(k)}{\hat{L}_d(k)} + \frac{T_s u_d(k)}{\hat{L}_d(k)} \\ \hat{i}_q(k) - \frac{T_s(-p)\omega_r(k) \hat{i}_d(k) \hat{L}_d(k)}{\hat{L}_q(k)} - \frac{T_s R_s \hat{i}_q(k)}{\hat{L}_q(k)} + \frac{T_s u_q(k)}{\hat{L}_q(k)} - \frac{T_s \Psi_p p \omega_r(k)}{\hat{L}_q(k)} \\ \hat{L}_d(k) + T_s(\Theta_d(1) \hat{i}_q(k) \tilde{i_d}(k) + \Theta_d(1) \hat{i}_d(k) \tilde{i_q}(k) + \Theta_d(2) \tilde{i_d}(k) + \Theta_d(3) \tilde{i_q}(k)) \\ \hat{L}_q(k) + T_s\left(\Theta_q(1) \hat{i}_d(k) \tilde{i_q}(k) + \Theta_q(1) \hat{i}_q(k) \tilde{i_d}(k) + \Theta_q(2) \tilde{i_d}(k) + \Theta_q(3) \tilde{i_q}(k)\right) \end{bmatrix}. \tag{24}$$

with $\tilde{i_d}$ and $\tilde{i_q}$ as derivations (20) and (21) for the currents i_d and i_q and T_s as the sample time. The discrete nonlinear system equations in (24) are taken for the estimation of the a-priori states $\hat{x}^-(k+1)$ in the EKF in the prediction step. The initial values of $\hat{\mathbf{x}}^+(0)$ are given by the nominal values for L_d and L_q in the data sheet and a value which is not zero for the currents i_d and i_q. For the estimation of the a-priori states $\hat{\mathbf{x}}^-(k+1)$ in the prediction step, the EKF uses the a-posteriori estimation $\hat{\mathbf{x}}^+(k)$ of the last iteration. The electrical model is described by nonlinear system equations, which make it necessary for the estimation process of the EKF to derive the Jacobian matrix:

$$\mathbf{J}(k+1) = \begin{bmatrix} \frac{\partial i_d(k+1)}{\partial i_d(k)} & \frac{\partial i_d(k+1)}{\partial i_q(k)} & \frac{\partial i_d(k+1)}{\partial L_d(k)} & \frac{\partial i_d(k+1)}{\partial L_q(k)} \\ \frac{\partial i_q(k+1)}{\partial i_d(k)} & \frac{\partial i_q(k+1)}{\partial i_q(k)} & \frac{\partial i_q(k+1)}{\partial L_d(k)} & \frac{\partial i_q(k+1)}{\partial L_q(k)} \\ \frac{\partial L_d(k+1)}{\partial i_d(k)} & \frac{\partial L_d(k+1)}{\partial i_q(k)} & \frac{\partial L_d(k+1)}{\partial L_d(k)} & \frac{\partial L_d(k+1)}{\partial L_q(k)} \\ \frac{\partial L_q(k+1)}{\partial i_d(k)} & \frac{\partial L_q(k+1)}{\partial i_q(k)} & \frac{\partial L_q(k+1)}{\partial L_d(k)} & \frac{\partial L_q(k+1)}{\partial L_q(k)} \end{bmatrix}. \tag{25}$$

After calculating the Jacobian matrix by using the estimation results of the last iteration, we get the following 4×4 matrix for the electrical system:

$$\mathbf{J}(k+1) = \begin{bmatrix} 1 - T_s \frac{R_s}{\hat{L}_d(k)} & T_s \omega(k) \frac{\hat{L}_q(k)}{\hat{L}_d(k)} & J_{13} & T_s \omega(k) \frac{\hat{i}_q(k)}{\hat{L}_d(k)} \\ -T_s \omega(k) \frac{\hat{L}_d(k)}{\hat{L}_q(k)} & 1 - T_s \frac{R_s}{\hat{L}_q(k)} & -T_s \omega(k) \frac{\hat{i}_d(k)}{\hat{L}_q(k)} & J_{24} \\ J_{31} & J_{32} & J_{33} & J_{34} \\ J_{41} & J_{42} & J_{43} & J_{44} \end{bmatrix}. \tag{26}$$

For the sake of brevity, the elements $\mathbf{J}_{13}$ and $\mathbf{J}_{24}$ to $\mathbf{J}_{44}$ are not given in detail.

5. Decoupling MPC

The MPC structure requires the estimation of the parameters to realize a prediction using a linear, albeit time-varying, system and to preserve the convexity of the optimization problem. Thus also the proposed structure of the MPC must be adaptive, see Fig. 1. In (7), it can be seen that the d-portion influences the q-axis of the equation, just as the q-portion influences the d-axis in the opposite direction. This effect is called the cross-coupling effect and comes from the fact that a d-current leads to a pre saturation in the q-axis as well as a q-current leading to pre saturation in the d-axis. A good explanation for the consideration of the magnetic conditions is given in [52]. In [53] it was shown, that a feedforward action is necessary to decouple these cross coupled voltages (1) as well as (2) by feedforwarding the reverse directed voltages as in Fig. 1 with

$$u_{dff}(t) = -\omega(t)\hat{L}_q(t)\hat{i}_q(t) \tag{27}$$

and

$$u_{qff}(t) = \omega(t)(\hat{L}_d(t)\hat{i}_d(t) + \Psi_p), \tag{28}$$

with $\hat{i}_d$, $\hat{i}_q$, $\hat{L}_d$ and $\hat{L}_q$ as the estimated states of the EKF. As we can see in Fig. 1, the feedforward action needs to be adjusted to cancel out the interacting part of the model and realize this decoupled system. Due to the saturation behavior of the inductances, the estimation of these by the EKF becomes even more important to guarantee a good enough decoupling for the d- and q- axis. The advantages of decoupling in PMSMs are known, the geometric approach (see [54]) offers effective tools to realize a noninteracting control strategy. Applications of this can be seen in [54], in which an electromagnetic actuator is controlled using a decoupling structure.

5.1. MPC for constant torque and constant power region

Using this feedforward control, the following decoupled system is obtained:

$$\underbrace{\begin{bmatrix} \frac{di_d(t)}{dt} \\ \frac{di_q(t)}{dt} \end{bmatrix}}_{\dot{\mathbf{x}}(t)} = \underbrace{\begin{bmatrix} \frac{-R_s}{L_d(t)} & 0 \\ 0 & \frac{-R_s}{L_q(t)} \end{bmatrix}}_{\mathbf{A}(t)} \underbrace{\begin{bmatrix} i_d(t) \\ i_q(t) \end{bmatrix}}_{\mathbf{x}(t)} + \underbrace{\begin{bmatrix} \frac{1}{L_d(t)} & 0 \\ 0 & \frac{1}{L_q(t)} \end{bmatrix}}_{\mathbf{B}(t)} \underbrace{\begin{bmatrix} u_d(t) \\ u_q(t) \end{bmatrix}}_{\mathbf{u}_{mpc}(t)}. \tag{29}$$

Considering $k = nT_s$ and $k+1 = (n+1)T_s$, where T_s represents the sampling time and $n \in \mathbb{N}$, then the following expression can be obtained:

$$\begin{aligned} \mathbf{x}(k+1) &= \mathbf{A}_k \mathbf{x}(k) + \mathbf{B}_k \mathbf{u}_{mpc}(k) \\ y_h(k) &= \mathbf{H}_k \mathbf{x}(k), \end{aligned} \tag{30}$$

where $\mathbf{A}_k$ represents the discretization of the 2×2 diagonal block matrix $\mathbf{I} + T_s\mathbf{A}(t)$, matrix $\mathbf{B}_k$ represents, in the same way, the discretization of each block matrix of matrix $\mathbf{B}(t)$; and it results that ($\mathbf{B}_k = T_s\mathbf{B}(t)$), $\mathbf{x}(k)$ is the discrete state variable and matrix $\mathbf{H}_k$ is the output matrix, which determines the two currents i_d and i_q. If a prediction horizon has a length of N samples, then this leads to the prediction expressions as follows:

$$\hat{y}_h(k+1) = \mathbf{H}_k\mathbf{A}_k\mathbf{x}(k) + \mathbf{H}_k\mathbf{B}\mathbf{u}_{mpc}(k) \tag{31}$$

$$\hat{y}_h(k+2) = \mathbf{H}_k\mathbf{A}_k^2\mathbf{x}(k) + \mathbf{H}_k\mathbf{A}_k\mathbf{B}_k u_{mpc}(k) + \mathbf{H}_k\mathbf{B}_k\mathbf{u}_{mpc}(k+1), \tag{32}$$

$$\vdots$$

$$\begin{aligned} \hat{y}_h(k+N) \;=\; & \mathbf{H}_k\mathbf{A}_k^N\mathbf{x}(k) + \mathbf{H}_k\mathbf{A}_k^{N-1}\mathbf{B}_k\mathbf{u}_{mpc}(k) \\ & + \ldots + \mathbf{H}_k\mathbf{B}_k\mathbf{u}_{mpc}(k+N-1). \end{aligned} \tag{33}$$

Expressions (31), (32) and (33) can be summarized as follows:

$$\hat{\mathbf{Y}}_h(k) = \mathbf{G}_p\mathbf{x}(k) + \mathbf{F}_{1p}\mathbf{U}_{mpc}(k), \tag{34}$$

where

$$\hat{\mathbf{Y}}_h(k) = \begin{bmatrix} \hat{y}_h(k+1) \\ \hat{y}_h(k+2) \\ \vdots \\ \hat{y}_h(k+N) \end{bmatrix}, \tag{35}$$

and

$$\mathbf{U}_{mpc}(k) = \begin{bmatrix} \mathbf{u}_{mpc}(k) \\ \mathbf{u}_{mpc}(k+1) \\ \vdots \\ \mathbf{u}_{mpc}(k+N-1) \end{bmatrix} \tag{36}$$

where the matrix $\mathbf{G}_p$ and the matrix $\mathbf{F}_{1p}$ are given by:

$$\mathbf{G}_p = \begin{bmatrix} \mathbf{H}_k\mathbf{A}_k \\ \mathbf{H}_k\mathbf{A}_k^2 \\ \vdots \\ \mathbf{H}_k\mathbf{A}_k^N \end{bmatrix}, \quad \mathbf{F}_{1p} = \begin{bmatrix} \mathbf{H}_k\mathbf{B}_k & \mathbf{0} & \dots & \mathbf{0} \\ \mathbf{H}_k\mathbf{A}_k\mathbf{B}_k & \mathbf{H}_k\mathbf{B}_k & \dots & \mathbf{0} \\ \vdots & \vdots & & \vdots \\ \mathbf{H}_k \sum_{i=1}^{N-1} \mathbf{A}_k^i\mathbf{B}_k & \mathbf{H}_k \sum_{i=1}^{N-2} \mathbf{A}_k^i\mathbf{B}_k & \dots & \mathbf{H}_k\mathbf{B}_k \end{bmatrix}. \tag{37}$$

Once a cost function is defined as follows:

$$J = \frac{1}{2}\sum_{j=1}^{N}\Big(\mathbf{y_d}(k+j) - \hat{\mathbf{y}}_h(k+j)\Big)^{\mathrm{T}}\mathbf{Q}_p\Big(\mathbf{y_d}(k+j) - \hat{\mathbf{y}}_h(k+j)\Big) + \sum_{j=1}^{N}\Big(\mathbf{u}_{mpc}(k+j)\Big)^{\mathrm{T}}\mathbf{R}_p\mathbf{u}_{mpc}(k+j), \tag{38}$$

$\mathbf{Q}_p$ and $\mathbf{R}_p$ are diagonal and positive weight matrices, then

$$\mathbf{H}_k = \begin{bmatrix} 1 & 0 \\ 0 & 1 \end{bmatrix} \tag{39}$$

is the matrix that selects currents i_d and i_q as outputs, then

$$\hat{\mathbf{Y}}_d(k+j) = \begin{bmatrix} \hat{i}_{dd}(k+j) \\ \hat{i}_{qd}(k+j) \end{bmatrix} \tag{40}$$

represents the desired outputs and

$$\hat{\mathbf{Y}}_h(k+j) = \begin{bmatrix} \hat{i}_d(k+j) \\ \hat{i}_q(k+j) \end{bmatrix} \tag{41}$$

represents the predicted outputs. Note that, in our specific control strategy, the desired currents are not available and thus should be predicted from the measured ones, as follows:

$$\hat{\mathbf{Y}}_d(k+j) = \begin{bmatrix} \hat{i}_{dd}(k+j) \\ \hat{i}_{qd}(k+j) \end{bmatrix} = \mathbf{G}_p \begin{bmatrix} \hat{i}_{dd}(k) \\ \hat{i}_{qd}(k) \end{bmatrix}. \tag{42}$$

Because of the convexity of the optimization problem (see [55]), the solution minimizing the cost function defined in (A.3) can be calculated with

$$\frac{\partial J}{\partial \mathbf{U}_{mpc}} = 0. \tag{43}$$

The unique optimal vector solution is as follows:

$$\tilde{\mathbf{U}}_{mpc} = (\mathbf{F}_{1p}^{\mathrm{T}}\mathbf{Q}_p\mathbf{F}_{1p} + \mathbf{R}_p)^{-1}\Big(\mathbf{F}_{1p}^{\mathrm{T}}\mathbf{Q}_p\big(\hat{\mathbf{Y}}_d(k+j) - \mathbf{G}_p x(k)\big)\Big). \tag{44}$$

It worthwhile to recall that $\hat{\mathbf{Y}}_d(k+j)$ represents the desired $i_d(k+j)$ and $i_q(k+j)$ currents calculated by the first sample of the desired current from the desired torque through matrix $\mathbf{G}_p$, see (42). It is to recall, see [55], that $\mathbf{G}_p x(k)$ represent the predicted currents calculated through matrix $\mathbf{G}_p$ from the measured ones.

Remark 1. Once the system is decoupled through the cancellation of the coupling nonlinearities thanks the decoupling action, the resulting system is a linear one and therefore, the optimization problem becomes a convex one. Eq. (44) states the unique solution of this optimization problem. Within this framework, the KF plays a crucial role by ensuring a satisfactory identification of parameters and states for the elimination of the coupling nonlinearity between the two dynamics. Consequently, it enables effective decoupling and an adequate suppression of the nonlinearity.

Remark 2. The cost function defined in (38) clearly depends on the length of the horizon. It is also known, see [55], that longer prediction and control horizons guarantee accurate solution. Nevertheless, the convexity of the solution does not depend on the

length of it. Moreover, longer horizons imply heavy computation costs. In this sense a compromise must be considered. In electrical systems, due to the relative short sampling time, typically a forecast for a period of a few samples is taken into account.

For more details related to this MPC, see [55].

6. Stability analysis for PI-MPC in constant power region

In this section, only the PI-MPC structure is considered in the analysis of stability. In fact, in the literature, see for example [11], an analysis of stability based on passivity is proposed for PMSM controlled by PI-PI current controllers. The MPC for the constant power region uses the same structure as for the constant torque region, even though the control is in the nonlinear region. This is due to the fact that the EKF estimate for the inductance provides a sufficiently accurate decoupling with the feedforward control. This underlines the importance of the presence of the EKF. Saturation states occur very frequently in applications, as explained. Basically, two types of saturations can occur: Input saturations and state saturations. The former are functional saturations that are very often imposed by the user to protect the machine from high voltages. The latter are physical limitations of the machines in terms of magnetic saturations. In the presence of input saturation, an anti-windup structure is used at the level of the PI reference governor and the $PI_{d/q}$ regulator to avoid windup. As already explained, an anti-windup is a control structure which allows to avoid that the integral action of a controller can generate overshoot as well as instability. Considering the following PI reference governor with an anti-windup structure:

$$i_{dd}(t) = K_P e(t) + K_I \int_0^t e(\tau) d\tau + A_w(t) \tag{45}$$

in which

$$e(t) = U_{max} - \omega(t)\sqrt{\psi_q^2(t) + (L_d(t) i_d(t) + \Psi_p)^2}, \tag{46}$$

where U_{max} is the maximal allowable voltage, i_{qd} is the q current that guarantees the required torque, and ω is the constant angular electric velocity corresponding to the fixed setting. Function A_w is the anti-windup signal with

$$A_w(t) = K_b\left(i_{dd}^*(t) - K_p(e(t)) - K_i \int_0^t e(\tau) d\tau\right), \tag{47}$$

where

$$i_{dd}^*(t) = \begin{cases} i_{dd}(t) & if \quad i_{dd}(t) < Sat_{out} \\ Sat_{out} & if \quad i_{dd}(t) \geq Sat_{out}, \end{cases} \tag{48}$$

where Sat_{out} is the constant of the saturation level of the controller output, which corresponds to the saturation level of the controller current output reflecting the saturation of the voltage input, and $K_b \in [0, \ 1)$ is a constant to be set. Note that the operating range of the power constant is characterized by $e(t) < 0$. If we consider the decoupled system described in (29), the following proposition holds which guarantees the robust asymptotic stability of the control law under the condition of flux weakening.

Remark 3. A preliminary and general analysis of the stability aspects concerning MPC with respect to the weighted matrices $\mathbf{Q}_p$, $\mathbf{R}_p$ is also considered in [56]. A sufficient asymptotic stability condition for the time-varying linear system derived using the Lyapunov approach, see [57] pages 114–115, is given by the eigenvalues λ_{t_i} of matrix $\mathbf{A}_k + \mathbf{A}_k^T$. This condition is $\|\lambda_{t_i}\| < 1$ for $i = 1, 2, \dots, n$. In addition, the eigenvalues of $\mathbf{A}_k^T$ are the same as the eigenvalues of $\mathbf{A}_k$ due to the diagonal form of the transition matrices in (29). This implies that $\mathbf{A}_k + \mathbf{A}_k^T = 2\mathbf{A}_k$ and that $\|\lambda_{t_i}\|$ of $\mathbf{A}_k + \mathbf{A}_k^T$ equals $2\|\lambda_{t_j}\|$ for $j = 1, 2, \dots, n$ for the eigenvalues of $\mathbf{A}_k$.

Theorem 1. *Let us consider the systems defined by the diagonal transition matrices (29) under the hypotheses (B.4) and (B.5) of the proposition given in the Appendix, for both non-saturating and saturating inputs, if*

$$\|\mathbf{A}_k\|_2 = 2\sqrt{\max_i \lambda_i(\mathbf{A}_k^T \mathbf{A}_k)}, \tag{49}$$

then

$$\lim_{k \to \infty} i_q(k) = i_{qd}(k) \tag{50}$$

and in particular

$$\lim_{k \to \infty} i_d(k) = i_{dd}(k). \tag{51}$$

Proof. The proof of the theorem is derived directly by the two propositions in Appendix.

Theorem 2. *Let the error function $e(t)$ in case $e(t) < 0$ be defined as in (46). For $K_P > 0$ and $K_I > 0$ under the hypothesis (B.4) and (B.5) of the proposition reported in the Appendix, in case of non input saturation as well as in case of input saturation, with hypothesis*

$$L_d(t) i_d(t) + \Psi_p > 0, \tag{52}$$

and

$$\|\mathbf{A}_k\|_2 = 2\sqrt{\max_i \lambda_i(\mathbf{A}_k^T \mathbf{A}_k)}, \tag{53}$$

then

$$\lim_{t\to\infty} e(t) = 0 \tag{54}$$

for each L_d, L_q, R_s.

Proof. Let consider the following Lyapunov function candidate:

$$V(e(t)) = \frac{1}{2}e^2(t), \tag{55}$$

then

$$\frac{dV(e(t))}{dt} = e(t)\frac{de(t)}{dt} = e(t)\frac{de(t)}{di_d(t)}\frac{di_d(t)}{dt}, \tag{56}$$

where, because of the decoupled structure of the controlled system, the following property is applied:

$$\frac{de(t)}{di_q(t)}\frac{di_q(t)}{dt} = 0, \tag{57}$$

$$\begin{aligned}\frac{de(t)}{dt} &= -\dot{\omega}(t)\sqrt{\psi_q^2(t) + (L_d(t)i_d + \Psi_p)^2} \\ &\quad - \frac{\omega(t)[2\psi_q(t)\dot{\psi}_q(t) + 2\psi_d(t)\dot{\psi}_d(t) + 2\Psi_p\dot{\psi}_d(t)]}{2\sqrt{\psi_q^2(t) + (\psi_d(t) + \Psi_p)^2}}.\end{aligned} \tag{58}$$

It is because of the decoupling structure of the model in (29)

$$\frac{d\psi_q(t)}{dt} = \frac{d\psi_q(t)}{di_d(t)}\frac{di_d(t)}{dt} = 0 \tag{59}$$

and $L_d(t)i_d(t)$, then

$$\frac{d\psi_d(t)}{dt} = \frac{d\psi_d(t)}{di_d(t)}\frac{di_d(t)}{dt} = \left(L_d(t) + \frac{L_d(t)}{di_d(t)}i_d(t)\right)\frac{di_d(t)}{dt}, \tag{60}$$

where $L_{d_{Diff.}}(t) = L_d(t) + \frac{L_d(t)}{di_d(t)}i_d(t) > 0$ is called Differential Inductance".[1] It follows that:

$$\begin{aligned}\frac{de(t)}{dt} &= -\dot{\omega}(t)\sqrt{\psi_q^2(t) + (L_d(t)i_d(t) + \Psi_p)^2} \\ &\quad - \frac{\omega(t)[2L_{d_{Diff.}}(t)(\psi_d(t) + \Psi_p)\frac{di_d(t)}{dt}]}{2\sqrt{\psi_q^2(t) + (\psi_d(t) + \Psi_p)^2}}.\end{aligned} \tag{61}$$

From (45), then

$$\frac{di_{dd}(t)}{dt} = K_p\dot{e}(t) + K_i e(t) + \dot{A}_w(t), \tag{62}$$

and in accordance with the definition of A_w in (47), the following expression is obtained:

$$K_p(1 - K_b)\dot{e}(t) + K_I(1 - K_b)e(t) = \frac{di_{dd}(t)}{dt}. \tag{63}$$

Combining (63) with (61) and considering the results of propositions (B.4) and (B.5) reported in the Appendix, then

$$\lim_{t\to\infty} i_d(t) = i_{dd}(t), \tag{64}$$

then the following expression is obtained:

$$D(t) = \sqrt{(L_q(t)i_q(t))^2 + (L_d(t)i_d(t) + \Psi_p)^2} > 0 \tag{65}$$

and it follows:

$$\dot{e}(t) = -\dot{\omega}(t)D(t) - \frac{\omega(t)2L_{d_{Diff}}(t)}{2D(t)}E(t), \tag{66}$$

[1] The differential inductance may indicate the effects of saturation. The additional term $\frac{L_d(t)}{di_d(t)}i_d(t) < 0$ depends on the shape of the curve $L_d(t)i_d(t)$ and becomes larger at higher currents.

where

$$E(t) = [(\psi_d(t) + \Psi_p)(K_p(1 - K_b)\dot{e}(t) + K_I(1 - K_b)e(t))]. \tag{67}$$

If

$$F(t) = \frac{\omega(t)2L_{d_{Diff}}(t)}{2D(t)} > 0 \tag{68}$$

then

$$\dot{e}(t)[1 + F(t)(\psi_d(t) + \Psi_p)(K_p(1 - K_b))] = \\ -\dot{\omega}(t)D(t) - F(t)K_I(1 - K_b)(\psi_d(t) + \Psi_p)e(t) \tag{69}$$

and it follows:

$$\dot{e}(t) = \frac{-\dot{\omega}(t)D(t) - F(t)K_I(1 - K_b)(\psi_d(t) + \Psi_p)e(t)}{[1 + F(t)(\psi_d(t) + \Psi_p)(K_p(1 - K_b))]} \tag{70}$$

and multiplying (70) by e(t) to obtain expression $\dot{e}(t)e(t)$, the following expression is obtained:

$$\frac{dV(e(t))}{dt} = \frac{-\dot{\omega}(t)D(t)}{[1 + F(t)(\psi_d(t) + \Psi_p)(K_p(1 - K_b))]} \\ - \frac{F(t)K_I(1 - K_b)(\psi_d(t) + \Psi_p)e^2(t)}{[1 + F(t)(\psi_d(t) + \Psi_p)(K_p(1 - K_b))]}. \tag{71}$$

It is straightforward to see that for $K_I > 0$ and $K_P > 0$ it follows:

$$\frac{dV(e(t))}{dt} < 0. \tag{72}$$

In fact, from hypothesis $L_d(t)i_d(t) + \Psi_p > 0$ and considering that, because of the limited desired torque T_d and a limited possible load torque T_l with the following mechanical model

$$J\dot{\omega}(t) = T_d(t) - T_l(t) - f(\omega) \tag{73}$$

in which J represents the inertia of machine and function $f(\omega)$ its the nonlinear friction model, it results $|\dot{\omega}| < M$ and thus $|\frac{\dot{\omega}}{p}| < M$ where M is a real value with $M < \infty$.

It is sufficient to choose $K_I > 0$ large enough and $K_p > 0$ to obtain the asymptotic stability in accordance with Lyapunov' stability concept. □

Remark 4. Proposition 2 states that for a given $K_P > 0$ and $K_I > 0$ a PI control guarantees the robust asymptotic stability of the all control structure under flux weakening condition with respect to L_d, L_q, R_s. The sufficient conditions stated by (B.4) and (B.5) of the Appendix are conditions to be satisfied the weight parameters of matrices $\mathbf{Q}_p$ and $\mathbf{R}_p$ of MPC. Parameter $K_P > 0$ large enough guarantees a rapid convergence of $e(t)$ to zero. The hypothesis $L_d(t)i_d(t)+\Psi_p > 0$ is a typical structural condition very often satisfied in PMSM as in the proposed experimental setup.

Remark 5. Condition on matrix $\mathbf{R}_p$ is quite straightforward to be satisfied. In fact, for instance a choice of a diagonal matrix for $\mathbf{R}_p$ with large diagonal elements represents a suitable choice. Once a suitable matrix $\mathbf{R}_p$ is obtained to satisfy, thanks to the particular diagonal structure of matrices $\mathbf{A}_k$ and $\mathbf{B}_k$, because of the decoupling control action, also the choice of matrix $\mathbf{Q}_p$ results to be straightforward.

7. Measured results in the presence of saturations

The measurements were taken with a HIL402 system from Typhoon HIL. The nonlinear PMSM machine model of the HIL402 schematic software provides the course of the current dependence inductance. This helps to compare the estimated inductance with the real inductance curve of the PMSM. Both the non-linear PMSM machine model and the traction inverter are simulated in a quasi-real-time environment. The switches used by Typhoon HIL within the modulation process of the inverter are ideal. The use of this type of switch means that there is no tendency to unphysical behavior, as can be the case with model approaches with simplified equivalents. In order to reproduce reality in as much detail as possible, the switches were parameterized with off and delay times and the losses were taken into account. The basis for this is the data sheet for the SKiM459GD12E4 IGBT module. The control was programmed in Simulink and then compiled into C-code. The code then runs as an embedded C-function within the FPGA of the HIL402. In Fig. 3, the control setup for the taken measurements is shown, while Fig. 1 shows the model-based system simulation setup for the simulation with MPC. The measurements were made with two different control concepts. Both control concepts exhibited input saturation in the form of a limit, which was set to 1 and −1, respectively, due to the normalization in both control concepts. There is a state saturation in the machine, too, by taking into account the saturated characteristic of the inductance. Both saturation types, input and state saturation, are given for constant torque as well as for the constant power region, where PI reference governor provides a negative i_d reference. The characteristic curve of the PMSM is given in Fig. 4 and gives

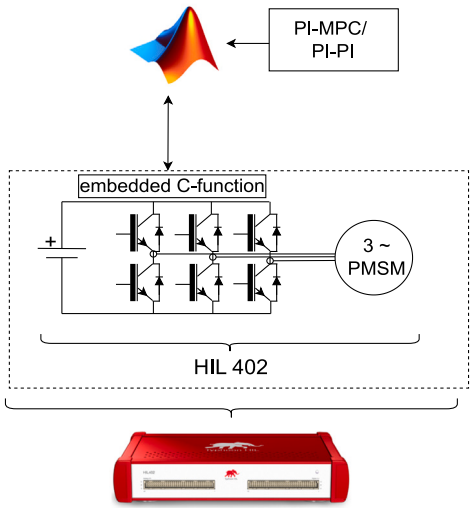

Fig. 3. HIL control setup.

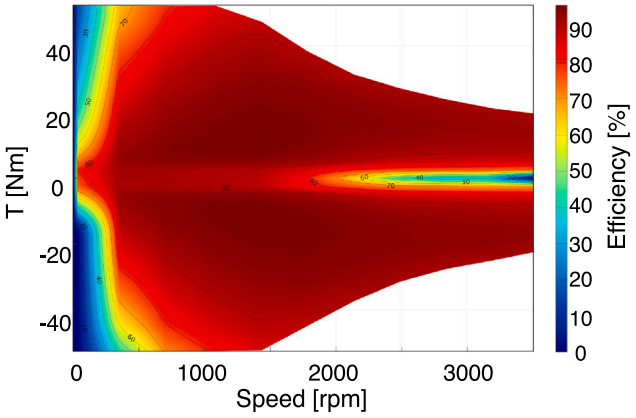

Fig. 4. Efficiency map of the PMSM under test.

information about the corner and the maximum speed as well as the permitted possible torque. The power rating of the PMSM is 10 kW. The following measurements show a comparison between a PI-PI controller, where the PI control loop is calculated according to the optimum amount, and the introduced PI-MPC control structure. The design of the PI controller for current control was done according to the optimum amount and decoupling the d axis and q axis, which is a valid approach for torque control, according to [47] or [53]. The PI control is set up adaptive together with the input of the estimated inductance out of the EKF, as the PMSM is operated in the non-linear range. The results were considered for two different regions, the constant torque as well as the constant power region.

7.1. Constant torque region

The constant torque region is characterized by the fact, that control takes place at the current limit and exceeding the maximum permissible voltage is generally not possible. When using a PMSM with surface mounted magnets respectively an isotropic machine, the field-forming current i_d is regulated to 0 in this range. This means that the PI reference governor for the field-weakening current is regulated to zero by the Sigmoid function in this region. The measurements in Figs. 5–10 were taken for the constant torque region, with a speed of 60 rad/sec. As it can be seen in Fig. 4, the maximum possible torque is given with 47 Nm for that speed. The decoupling of the $d-$ and q-axis was transmitted for the PI controller as well as for the MPC by means of an EKF. This allowed the most accurate decoupling possible to be generated for both control strategies. Fig. 17 shows the estimate of the inductance versus the current-dependent actual inductance. A slight bias can be seen here at the beginning of the estimation, when the impressed current is close to 0. This makes decoupling at this point more difficult for the MPC. The measurements in constant torque region were each recorded for the same torque jumps at a stable speed of 60 rad/sec. Fig. 5 as well as Fig. 6 show the results of the direct

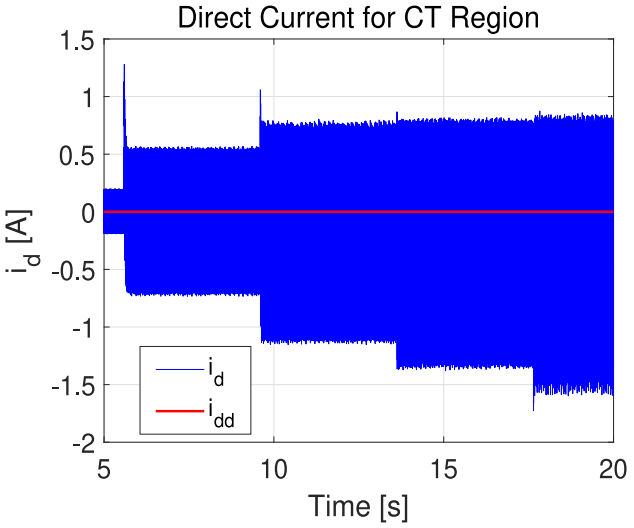

Fig. 5. Direct current with PI-PI for constant torque region.

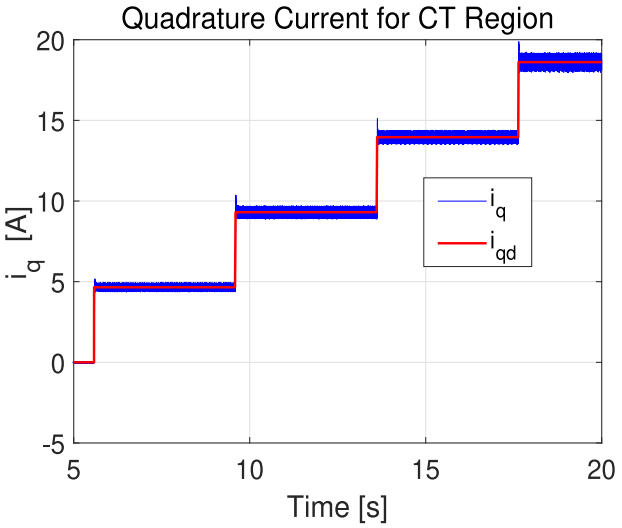

Fig. 6. Quadrature current with PI-PI for constant torque region.

current i_d as well as the quadrature current i_q. The direct current i_d oscillates close to 0. It can be seen that a small overshoot occurs in both current curves, what leads to the overshoot in Fig. 7, where the electromagnetic torque for the PI control in constant torque region is presented. The resulting overshoot leads significantly to the error described in Table 1. Compared to the results from the MPC, stationary accuracy is achieved due to the integral component, whereas with the MPC in Figs. 8 and 9, a gap between the setpoint and actual value for the currents i_d and i_q remains. The bias is largest where the estimate for the inductances in Fig. 17 also remains the least accurate. This also can be seen in the resulting torque for the PI-MPC in constant torque region in Fig. 10. Nevertheless, the error of the PI-MPC remains behind the resulting error from the PI-PI control. The proportional behavior of the MPC is shown to be advantageous compared to the PI controller.

7.2. Constant power region

The constant power region is characterized by control at the voltage limit. In order to be able to increase the speed further, but at the same time not to exceed the maximum permissible voltage, a negative d- current component must be impressed here. In this range, the field-weakening controller or the controller referred to here as the PI reference governor is used. This ensures that the negative d-current component is provided and thus that the maximum permissible voltage is maintained. The reference governor is a PI controller which provides the corresponding d-current by measuring the voltages. Fig. 1 shows the setup of the PI-MPC and

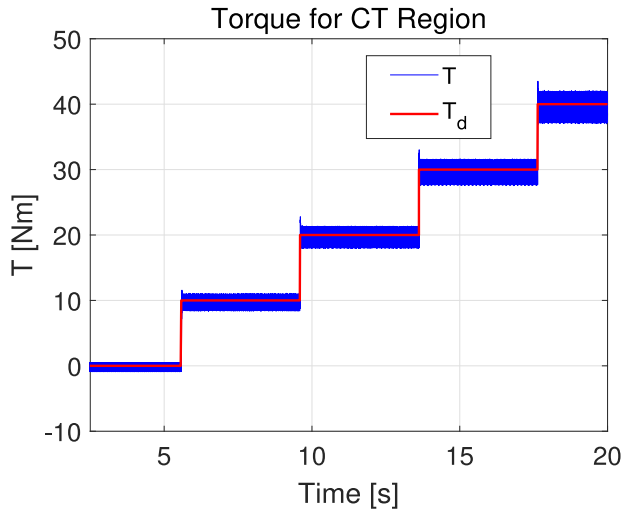

Fig. 7. Torque with PI-PI for constant torque region.

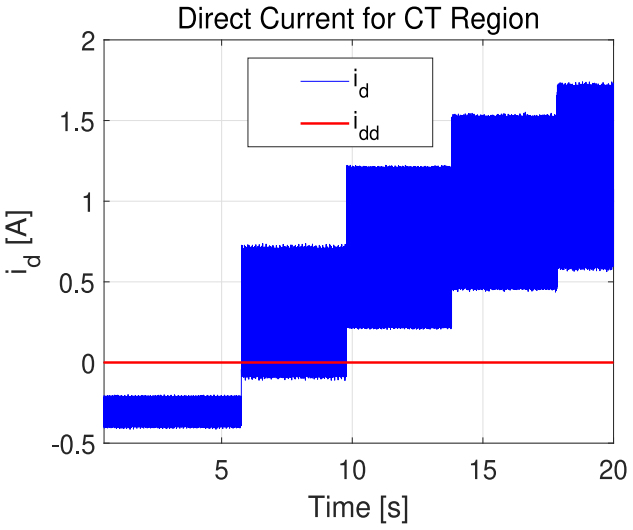

Fig. 8. Direct current with PI-MPC for constant torque region.

PI-PI control for constant power region, in the dashed section the PI reference governor. The measurements for constant power region were taken for a speed of 250 rad/sec. The corner speed of the electrical machine is defined at 159 rad/sec, the maximum speed is at 390 rad/sec. This means that the values were recorded in a range where field weakening becomes necessary with the addition of a negative d-current component. Again, the decoupling of the $d-$ and q-axis was transmitted for both control algorithms by means of an EKF. Figs. 11 and 14 show the recorded currents for the negative i_d current component. The overshoot behavior of the $d-$ current controlled by the PI controller and the PI reference governor is clearly visible in Fig. 11. Comparing both setpoint curves of the $d-$ current components, it can be seen that when using the PI controller, the setpoint input had to be set significantly slower, as the control process would otherwise have provoked too much overshoot. The MPC controller, on the other hand, can work with very high dynamics even without overshoot, since only the proportional component has an effect here. Compared to the constant torque region, the bias typical for the PI-MPC seems to be reduced and the PI reference governor has a positive influence on the steady-state accuracy for the MPC. Fig. 12 shows the quadrature current with the PI control and the PI reference governor. Compared to the results for the quadrature current i_q with PI-MPC in Fig. 15, the oscillation is higher for the smaller setpoints with PI-PI control than for the results with PI-MPC. The results for the torque with the PI-PI control in Fig. 13 show some oscillation around setpoint but no overshoot. Compared to the results for the torque measurements by the usage of the PI-MPC in Fig. 16, the oscillation is less for the PI-MPC, which can be seen in the resulting error in Table 1.

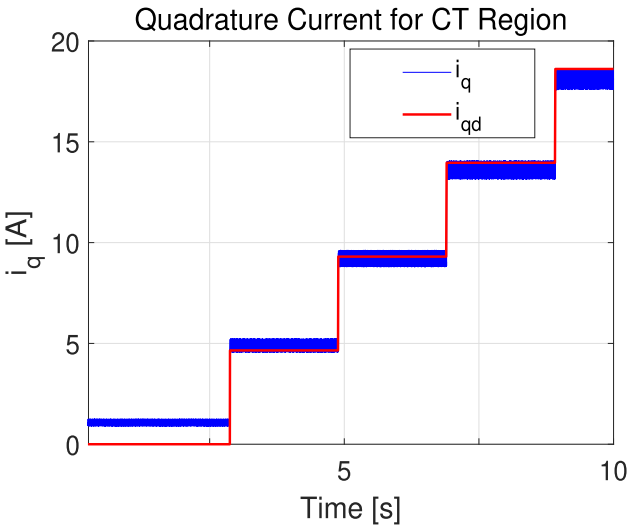

Fig. 9. Quadrature current with PI-MPC for constant torque region.

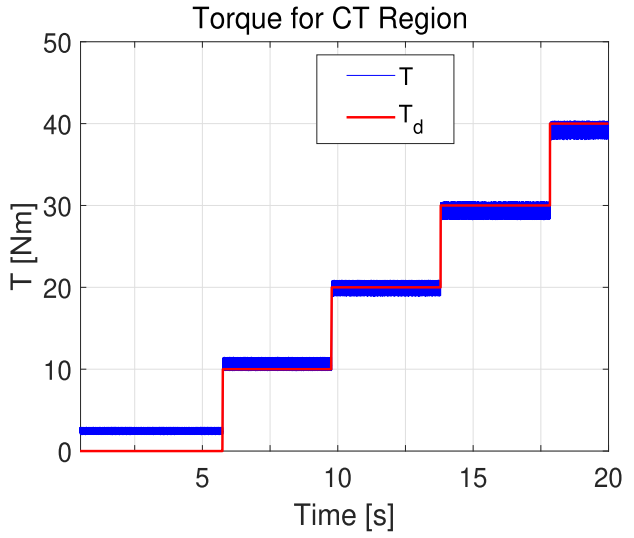

Fig. 10. Torque with PI-MPC for constant torque region.

Table 1
Failure of resulting torque ($E = \frac{1}{T}\int_0^T e(\tau)^2 d\tau$).

Type	PI-PI (failure)	PI-MPC (failure)
Constant torque region	42	40
Constant power region	35	15

With the failure

$$E = \frac{1}{T}\int_0^T e(\tau)^2 d\tau, \tag{74}$$

in which function $e(\tau)$ represents the difference between the desired and the obtained torque and T is a testing time horizon. The results are obtained with the following matrices for MPC to tune the EKF: measurement noise matrix

$$\mathbf{R}_w = \begin{bmatrix} 10 & 0 \\ 0 & 10 \end{bmatrix}, \tag{75}$$

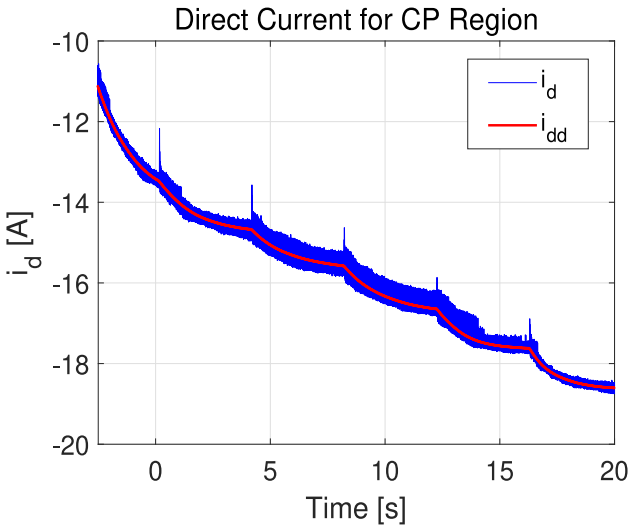

Fig. 11. Direct current with PI-PI for constant power region.

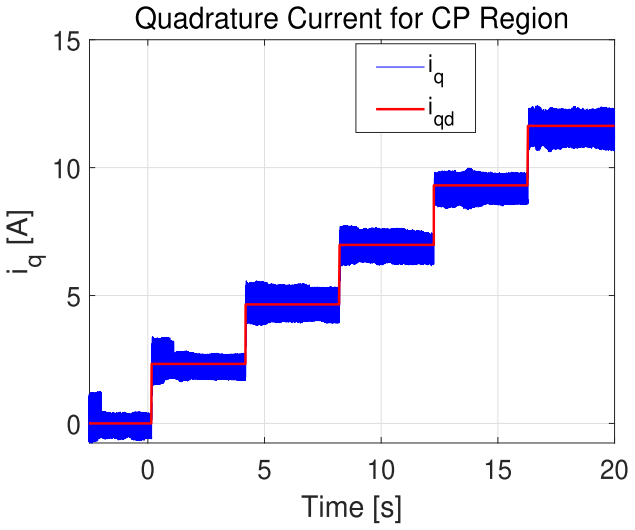

Fig. 12. Quadrature current with PI-PI for constant power region.

process noise matrix

$$\mathbf{Q} = \begin{bmatrix} 1e1 & 0 & 0 & 0 \\ 0 & 1e2 & 0 & 0 \\ 0 & 0 & 1e-7 & 0 \\ 0 & 0 & 0 & 1e-7 \end{bmatrix} \tag{76}$$

and the following initial a posteriori error covariance matrix

$$\mathbf{P_0} = \begin{bmatrix} 1 & 0 & 0 & 0 \\ 0 & 1 & 0 & 0 \\ 0 & 0 & 1e-3 & 0 \\ 0 & 0 & 0 & 1e-3 \end{bmatrix}. \tag{77}$$

Remark 6. Note that the results shown in Table 1 depend on the tuning parameters of both control strategies, inner loop PI and inner loop MPC. In the case of saturations, it is almost impossible to find satisfying tuning values to reduce the tracking error for the PI control, even in the case of adaptive tuning parameters. Recall that in the case of adaptive tuning parameters of the PI controller,

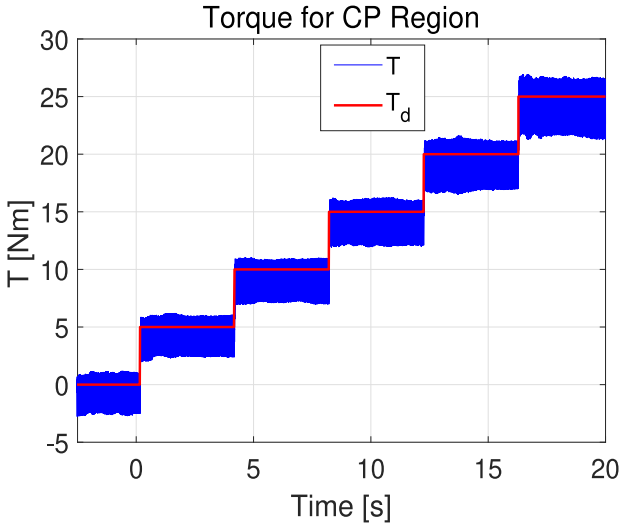

Fig. 13. Torque with PI-PI for constant power region.

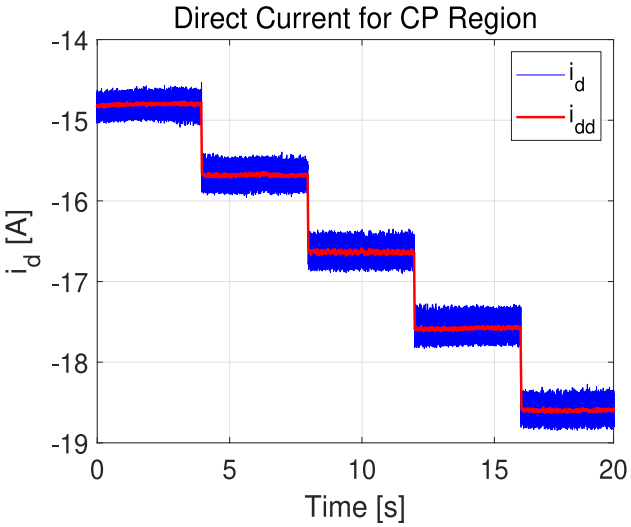

Fig. 14. Direct current with PI-MPC for constant power region.

the integral part is proportional to the inductance and thus it is reduced proportionally in the case of inductance saturation due to the increasing of the currents. In fact, we can say, that a comparison of different control techniques in order to show superiority of one control type is barely possible, as every control type has its advantages and drawbacks. The pure PI control for example, has no model based structure, what makes it less dynamic, but on the other hand makes it very easy to implement. In our paper, we have chosen the PI-PI-control together with feedforward structure as a comparison, as this control type is used very often for PMSM control. The aim was, to give a comparison to the state of the art, which in our case is the PI-PI control.

Remark 7. The importance of correctly tuning the $\mathbf{Q}$, which is the covariance matrix of the process noise and $\mathbf{R}_w$ as the covariance matrix of the measurement noise, should also be emphasized. The importance of tuning these matrices results from the fact that they have a decisive influence on the quality of the estimation of the EKF and thus on the maintenance of decoupling and hence stability and accuracy. In case of a linear observer with a linear systems and a linear controller, the tuning matrices $\mathbf{Q}$ and $\mathbf{R}_w$ are more easy to be tuned thank also to the separability principle, see [58–60]. To tend to this scenario, a decoupling of the system with its corresponding cancellation of the nonlinear part of the electrical dynamics is proposed together with an EKF which represents a linearization of the observer structure based on the KF.

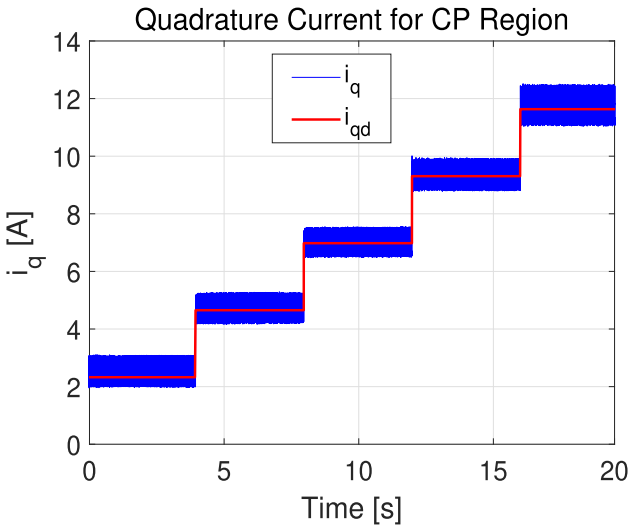

Fig. 15. Quadrature current with PI-MPC for constant power region.

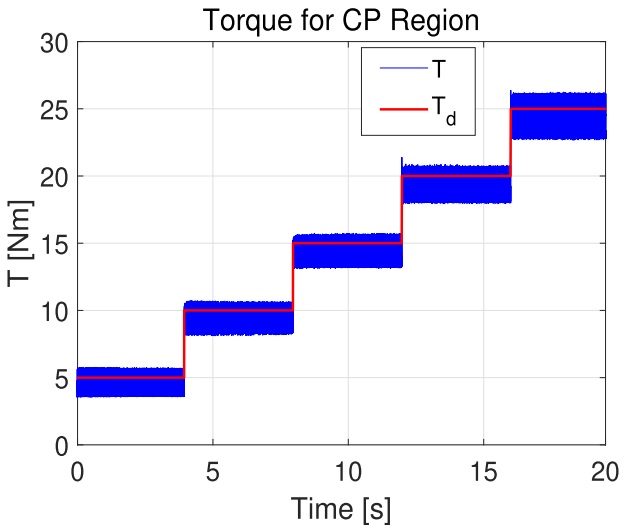

Fig. 16. Torque with PI-MPC for constant power region.

8. Conclusion

This paper shows a comparison of two different control methods for a permanent magnet synchronous machine control and considers the general problem of torque control in different working regions. The first control method considers a proportional integral control structure in the inner and outer loop, which is typically used in permanent magnet synchronous machines for the problem of the torque control. The second method takes into account the torque control with a model predictive control in the inner loop and a proportional integral control structure in the outer loop. Both control strategies use an extended Kalman filter to estimate inductance of the machines. The estimation of such a parameter is extremely important in the case of saturated inductances that yield saturated states. Measurement results in the presence of input and state saturations, through the saturated inductance, show that model predictive control is working without overshoot in the currents, which leads to less power needed in input. The advantage of the combination of outer loop proportional integral control and inner loop model predictive control is particularly evident in the area of field weakening, where the proportional integral reference governor becomes more important due to the Sigmoid function and now takes over the setpoint specification for the field-weakening current i_d.

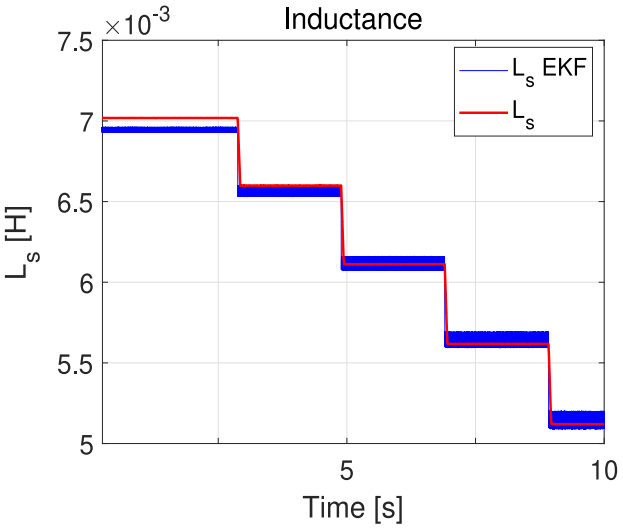

Fig. 17. Estimated inductance for a machine with nonlinear and saturated inductance.

CRediT authorship contribution statement

Tanja Zwerger: Conceptualization, Data curation, Formal analysis, Investigation, Methodology, Software, Validation, Visualization, Writing – original draft, Writing – review & editing. **Paolo Mercorelli:** Conceptualization, Data curation, Formal analysis, Funding acquisition, Investigation, Methodology, Project administration, Resources, Software, Supervision, Validation, Visualization, Writing – original draft, Writing – review & editing,.

Appendix A. An asymptotic stability sufficient constructive condition in MPC

Proposition 1. *Let us take the following discrete SISO linear system into consideration:*

$$\mathbf{z}(k+1) = \mathbf{A}_k \mathbf{z}(k) + \mathbf{B}_k u_{mpc}(k), \tag{A.1}$$

$$y(k) = \mathbf{H}_k \mathbf{z}(k), \tag{A.2}$$

which is obtained by a discretization of a linear continuous system using a sampling time which equals T_s. $u_{mpc}(k)$ represents the first element of the vector of the optimal solution as calculated in [55] for the MPC considering the following cost function:

$$J = \frac{1}{2}\sum_{j=1}^{N}\Big(\mathbf{y_d}(k+j) - \hat{\mathbf{y}}(k+j)\Big)^{\mathrm{T}}\mathbf{Q}_p\Big(\mathbf{y_d}(k+j) - \hat{\mathbf{y}}(k+j)\Big) + \sum_{j=1}^{N}\Big(\mathbf{u}_{mpc}(k+j-1)\Big)^{\mathrm{T}}\mathbf{R}_p\mathbf{u}_{mpc}(k+j-1), \tag{A.3}$$

where $\mathbf{y_d}(k+j)$, $j = 1, 2, \ldots, N$ is the output reference trajectory and N is the prediction horizon, and $\mathbf{Q}_p$ and $\mathbf{R}_p$ are diagonal and positive matrices. Furthermore, the solution minimizing performance index (A.3) may be obtained by solving:

$$\frac{\partial J}{\partial \mathbf{U}_{mpc}} = 0. \tag{A.4}$$

It is known for instance from [55] that the optimal solution is

$$\tilde{U}_{mpc}(k) = (\mathbf{F}_{1p}^{\mathrm{T}}\mathbf{Q}_p\mathbf{F}_{1p} + \mathbf{R}_p)^{-1}\mathbf{F}_{1p}^{\mathrm{T}}\mathbf{Q}_p\Big(\mathbf{Y}_{d_p}(k) - \mathbf{G}_p\mathbf{z}(k)\Big), \tag{A.5}$$

where $\mathbf{Y}_{d_p}(k)$ is the desired output column vector. Matrices $\mathbf{Q}_p$ and $\mathbf{R}_p$ are diagonal and positive defined. Under the hypothesis that system (A.5) is asymptotically stable, i.e. ($\|\mathbf{A}_k\|_2 < 1$), where

$$\|\mathbf{A}_k\|_2 = \sqrt{\max_i \lambda_i(\mathbf{A}_k^T\mathbf{A}_k)} \quad \text{for} \quad i = 1, 2, \ldots, n \in \mathbb{N}$$

represents the root of the maximal eigenvalue of matrix $\mathbf{A}_k^T\mathbf{A}_k$, then $\forall$ $\mathbf{R}_p$ diagonal and positive defined matrix such that

$$\|\mathbf{R}_p\|_2 > \frac{\|\mathbf{B}_k\mathbf{F}_{1p}^{\mathrm{T}}\mathbf{Q}_p\mathbf{G}_p\|_2}{1 - \|\mathbf{A}_k\|_2} \tag{A.6}$$

and

$$\left\|\mathbf{A}_k - \mathbf{B}_k(\mathbf{F}_{1p}^{\mathrm{T}}\mathbf{Q}_p\mathbf{F}_{1p} + \mathbf{R}_p)^{-1}\mathbf{F}_{1p}^{\mathrm{T}}\mathbf{Q}_p\mathbf{G}_p\right\|_2 < \left\|\mathbf{A}_k + \mathbf{B}_k(\mathbf{F}_{1p}^{\mathrm{T}}\mathbf{Q}_p\mathbf{F}_{1p} + \mathbf{R}_p)^{-1}\mathbf{F}_{1p}^{\mathrm{T}}\mathbf{Q}_p\mathbf{G}_p\right\|_2, \tag{A.7}$$

the system (A.1) results to be asymptotically stable.[2]

Proof. For one prediction step is considered, then, according to [55], it follows that:

$$\mathbf{F}_{1p} = \left[\mathbf{H}_k\mathbf{B}_k\right], \tag{A.8}$$

$$\mathbf{G}_p = \left[\mathbf{H}_k\mathbf{A}_k\right]. \tag{A.9}$$

Combining Eq. (A.1) with (A.5), this expression is obtained:

$$\mathbf{z}(k+1) = \mathbf{A}_k\mathbf{z}(k) + \mathbf{B}_k(\mathbf{F}_{1p}^{\mathrm{T}}\mathbf{Q}_p\mathbf{F}_{1p} + \mathbf{R}_p)^{-1}\mathbf{F}_{1p}^{\mathrm{T}}\mathbf{Q}_p\left(\mathbf{Y}_{d_p}(k) - \mathbf{G}_p\mathbf{z}(k)\right), \tag{A.10}$$

which is equivalent to write:

$$\begin{aligned}\mathbf{z}(k+1) = {} & \left(\mathbf{A}_k - \mathbf{B}_k(\mathbf{F}_{1p}^{\mathrm{T}}\mathbf{Q}_p\mathbf{F}_{1p} + \mathbf{R}_p)^{-1}\mathbf{F}_{1p}^{\mathrm{T}}\mathbf{Q}_p\mathbf{G}_p\right)\mathbf{z}(k) \\ & + \mathbf{B}_k(\mathbf{F}_{1p}^{\mathrm{T}}\mathbf{Q}_p\mathbf{F}_{1p} + \mathbf{R}_p)^{-1}\mathbf{F}_{1p}^{\mathrm{T}}\mathbf{Q}_p\mathbf{Y}_{d_p}(k).\end{aligned} \tag{A.11}$$

If

$$\|\mathbf{R}_p\|_2 > \frac{\|\mathbf{B}_k\mathbf{F}_{1p}^{\mathrm{T}}\mathbf{Q}_p\mathbf{G}_p\|_2}{1 - \|\mathbf{A}_k\|_2}, \tag{A.12}$$

considering that $\|\mathbf{R}_p\| > 0$,

$$\|\mathbf{A}_k\|_2 + \|\mathbf{R}_p\|_2^{-1}\|\mathbf{B}_k\mathbf{F}_{1p}^{\mathrm{T}}\mathbf{Q}_p\mathbf{G}_p\|_2 < 1, \text{and thus} \tag{A.13}$$

$$\|\mathbf{A}_k\|_2 + \left\|\mathbf{B}_k\mathbf{R}_p^{-1}\mathbf{F}_{1p}^{\mathrm{T}}\mathbf{Q}_p\mathbf{G}_p\right\|_2 < 1. \tag{A.14}$$

as a consequence it follows that:

$$\|\mathbf{A}_k\|_2 + \left\|\mathbf{B}_k(\mathbf{F}_{1p}^{\mathrm{T}}\mathbf{Q}_p\mathbf{F}_{1p} + \mathbf{R}_p)^{-1}\mathbf{F}_{1p}^{\mathrm{T}}\mathbf{Q}_p\mathbf{G}_p\right\|_2 < 1. \tag{A.15}$$

Considering the norm properties and condition (A.7), then

$$\begin{aligned}&\left\|\mathbf{A}_k - \mathbf{B}_k(\mathbf{F}_{1p}^{\mathrm{T}}\mathbf{Q}_p\mathbf{F}_{1p} + \mathbf{R}_p)^{-1}\mathbf{F}_{1p}^{\mathrm{T}}\mathbf{Q}_p\mathbf{G}_p\right\|_2 \\ &< \left\|\mathbf{A}_k + \mathbf{B}_k(\mathbf{F}_{1p}^{\mathrm{T}}\mathbf{Q}_p\mathbf{F}_{1p} + \mathbf{R}_p)^{-1}\mathbf{F}_{1p}^{\mathrm{T}}\mathbf{Q}_p\mathbf{G}_p\right\|_2 \\ &< \|\mathbf{A}_k\|_2 + \left\|\mathbf{B}_k(\mathbf{F}_{1p}^{\mathrm{T}}\mathbf{Q}_p\mathbf{F}_{1p} + \mathbf{R}_p)^{-1}\mathbf{F}_{1p}^{\mathrm{T}}\mathbf{Q}_p\mathbf{G}_p\right\|_2 < 1.\end{aligned} \tag{A.16}$$

To conclude

$$\left\|\mathbf{A}_k - \mathbf{B}_k(\mathbf{F}_{1p}^{\mathrm{T}}\mathbf{Q}_p\mathbf{F}_{1p} + \mathbf{R}_p)^{-1}\mathbf{F}_{1p}^{\mathrm{T}}\mathbf{Q}_p\mathbf{G}_p\right\|_2 < 1. \tag{A.17}$$

Condition (A.17) states that the eigenvalues of the controlled system described by (A.11) are all inside the complex unit circle and thus system (A.11) results to be asymptotically stable. □

Appendix B. The saturation case

Proposition 2. *Let us take the following discrete SISO linear system into consideration:*

$$\mathbf{z}(k+1) = \mathbf{A}_k\mathbf{z}(k) + \mathbf{B}_k U_{mpc}(k), \tag{B.1}$$

$$y(k) = \mathbf{H}_k\mathbf{z}(k), \tag{B.2}$$

and let U_{max} be a real value with

$$|U_{mpc}(k)| < U_{max} \quad \forall k, \tag{B.3}$$

[2] It is to notice that matrix $\mathbf{R}_p$ collapses in a scalar in case of one step prediction horizon, $\mathbf{R}_p = r$.

then (B.1) with the input saturation defined in (B.3) and controlled with the control law in (A.5) is asymptotically stable and its input avoids the saturation constraint if the following conditions are hold:

$$r = \|\mathbf{R}_p\|_2 > \max\left\{ \frac{\|\mathbf{B}_k\mathbf{F}_{1p}^{\mathrm{T}}\mathbf{Q}_p\mathbf{Y}_{d_p}(k)\|_2}{U_{max}} - \|\mathbf{F}_{1p}^{\mathrm{T}}\mathbf{Q}_p\mathbf{F}_{1p}\|_2, \quad \frac{\|\mathbf{B}_k\mathbf{F}_{1p}^{\mathrm{T}}\mathbf{Q}_p\mathbf{G}_p\|_2}{1-\|\mathbf{A}_k\|_2} \right\} \tag{B.4}$$

and

$$\begin{aligned} &\left\|\mathbf{A}_k - \mathbf{B}_k(\mathbf{F}_{1p}^{\mathrm{T}}\mathbf{Q}_p\mathbf{F}_{1p} + \mathbf{R}_p)^{-1}\mathbf{F}_{1p}^{\mathrm{T}}\mathbf{Q}_p\mathbf{G}_p\right\|_2 \\ &< \left\|\mathbf{A}_k + \mathbf{B}_k(\mathbf{F}_{1p}^{\mathrm{T}}\mathbf{Q}_p\mathbf{F}_{1p} + \mathbf{R}_p)^{-1}\mathbf{F}_{1p}^{\mathrm{T}}\mathbf{Q}_p\mathbf{G}_p\right\|_2. \end{aligned} \tag{B.5}$$

Proof. The demonstration is straightforward. In fact, just considering that

$$|U_{mpc}(k)| < U_{max} \quad \forall k$$

and thus, considering the input of the optimal predicted expression (A.11), it is enough that the following condition holds:

$$\left\|\mathbf{B}_k(\mathbf{F}_{1p}^{\mathrm{T}}\mathbf{Q}_p\mathbf{F}_{1p} + \mathbf{R}_p)^{-1}\mathbf{F}_{1p}^{\mathrm{T}}\mathbf{Q}_p\mathbf{Y}_{d_p}(k)\right\|_2 < U_{max}. \tag{B.6}$$

This can be written as

$$\begin{aligned} &\left\|\mathbf{B}_k(\mathbf{F}_{1p}^{\mathrm{T}}\mathbf{Q}_p\mathbf{F}_{1p} + \mathbf{R}_p)^{-1}\mathbf{F}_{1p}^{\mathrm{T}}\mathbf{Q}_p\mathbf{Y}_{d_p}(k)\right\|_2 \\ &< \left\|(\mathbf{F}_{1p}^{\mathrm{T}}\mathbf{Q}_p\mathbf{F}_{1p} + \mathbf{R}_p)^{-1}\right\|_2 \left\|\mathbf{B}_k\mathbf{F}_{1p}^{\mathrm{T}}\mathbf{Q}_p\mathbf{Y}_{d_p}(k)\right\|_2 < U_{max}. \end{aligned} \tag{B.7}$$

Considering that $\mathbf{R}_p$ and $\mathbf{F}_{1p}^{\mathrm{T}}\mathbf{Q}_p\mathbf{F}_{1p}$ are both positive scalars in case of one step of the prediction horizon, then

$$\left\|\mathbf{F}_{1p}^{\mathrm{T}}\mathbf{Q}_p\mathbf{F}_{1p} + \mathbf{R}_p\right\|_2 < \frac{\|\mathbf{B}_k\mathbf{F}_{1p}^{\mathrm{T}}\mathbf{Q}_p\mathbf{Y}_{d_p}(k)\|_2}{U_{max}}. \tag{B.8}$$

and thus, to guarantee asymptotic stability and anti saturation input of system (B.1), it follows:

$$r = \|\mathbf{R}_p\|_2 > \max\left\{ \frac{\|\mathbf{B}_k\mathbf{F}_{1p}^{\mathrm{T}}\mathbf{Q}_p\mathbf{Y}_{d_p}(k)\|_2}{U_{max}} - \|\mathbf{F}_{1p}^{\mathrm{T}}\mathbf{Q}_p\mathbf{F}_{1p}\|_2, \quad \frac{\|\mathbf{B}_k\mathbf{F}_{1p}^{\mathrm{T}}\mathbf{Q}_p\mathbf{G}_p\|_2}{1-\|\mathbf{A}_k\|_2} \right\}. \quad \square \tag{B.9}$$

References

[1] G. Mueller, B. Ponick, Grundlagen Elektrischer Maschinen, Wiley-VCH, Weinheim, 2006.

[2] G. Sturtzer, D. Flieller, J.-P. Louis, Reduction of torque undulation and extension of the Park's transformation applied to non-sinusoidal saturated synchronous motors, Math. Comput. Simulation 63 (3–5) (2003) 297–305, http://dx.doi.org/10.1016/s0378-4754(03)00077-6.

[3] E. Uygun, M. Hecquet, A. Tounzi, D. Depernet, V. Lanfranchi, S. Bruno, T. Tollance, Influence of the load angle on magnetic radial forces and torque ripple of a low power permanent magnet synchronous machine, Math. Comput. Simulation 184 (2021) 153–164, http://dx.doi.org/10.1016/j.matcom.2020.05.020.

[4] M. Karimi, M.A. Rostami, H. Zamani, Continuous control set model predictive control for the optimal current control of permanent magnet synchronous motors, Control. Eng. Pract. 138 (2023) 105590, http://dx.doi.org/10.1016/j.conengprac.2023.105590, URL https://www.sciencedirect.com/science/article/pii/S0967066123001594.

[5] Y. Liu, S. Cheng, B. Ning, Y. Li, Robust model predictive control with simplified repetitive control for electrical machine drives, IEEE Trans. Power Electron. 34 (5) (2019) 4524–4535, http://dx.doi.org/10.1109/TPEL.2018.2857837.

[6] W. Gui, J. Gao, C. Yang, T. Peng, C. Yang, Y. Han, Optimized FCS-MPCC based on disturbance feedback rejection for IPMSMs under demagnetization fault in high-speed trains, Control. Eng. Pract. 141 (2023) 105670, http://dx.doi.org/10.1016/j.conengprac.2023.105670, URL https://www.sciencedirect.com/science/article/pii/S0967066123002393.

[7] M. Bermudez, O. Gomozov, X. Kestelyn, F. Barrero, N.K. Nguyen, E. Semail, Model predictive optimal control considering current and voltage limitations: Real-time validation using OPAL-RT technologies and five-phase permanent magnet synchronous machines, Math. Comput. Simulation 158 (2019) 148–161, http://dx.doi.org/10.1016/j.matcom.2018.07.005.

[8] X. Sun, C. Hu, J. Zhu, S. Wang, W. Zhou, Z. Yang, G. Lei, K. Li, B. Zhu, Y. Guo, MPTC for PMSMs of EVs with multi-motor driven system considering optimal energy allocation, IEEE Trans. Magn. 55 (7) (2019) 1–6, http://dx.doi.org/10.1109/TMAG.2019.2904289.

[9] M. Wu, X. Sun, J. Zhu, G. Lei, Y. Guo, Improved model predictive torque control for PMSM drives based on duty cycle optimization, IEEE Trans. Magn. 57 (2) (2021) 1–5, http://dx.doi.org/10.1109/TMAG.2020.3008495.

[10] T. Englert, K. Graichen, Nonlinear model predictive torque control of PMSMs for high performance applications, Control. Eng. Pract. 81 (2018) 43–54, http://dx.doi.org/10.1016/j.conengprac.2018.08.023, URL https://www.sciencedirect.com/science/article/pii/S0967066118304854.

[11] R. Ortega, N. Monshizadeh, P. Monshizadeh, D. Bazylev, A. Pyrkin, Permanent magnet synchronous motors are globally asymptotically stabilizable with PI current control, Automatica 98 (2018) 296–301, http://dx.doi.org/10.1016/j.automatica.2018.09.031, URL https://www.sciencedirect.com/science/article/pii/S0005109818304564.

[12] Z. qiang Wu, C. hua Xu, Y. Yang, Adjustable PID control based on adaptive internal model and application in current shared control of multi inverters, J. Franklin Inst. 354 (7) (2017) 2699–2711, http://dx.doi.org/10.1016/j.jfranklin.2017.01.019.

[13] H. Li, B. Song, T. Chen, Y. Xie, X. Zhou, Adaptive fuzzy PI controller for permanent magnet synchronous motor drive based on predictive functional control, J. Franklin Inst. 358 (15) (2021) 7333–7364, http://dx.doi.org/10.1016/j.jfranklin.2021.07.024.
[14] J. Zhang, Design of a new PID controller using predictive functional control optimization for chamber pressure in a coke furnace, ISA Trans. 67 (2017) 208–214, http://dx.doi.org/10.1016/j.isatra.2016.11.006.
[15] K. Lu, W. Zhou, G. Zeng, W. Du, Design of PID controller based on a self-adaptive state-space predictive functional control using extremal optimization method, J. Franklin Inst. 355 (5) (2018) 2197–2220, http://dx.doi.org/10.1016/j.jfranklin.2017.12.034.
[16] A. Brosch, O. Wallscheid, J. Boecker, Long-term memory recursive least squares online identification of highly utilized permanent magnet synchronous motors for finite-control-set model predictive control, IEEE Trans. Power 38 (2) (2023) 1451–1467, http://dx.doi.org/10.1109/TPEL.2022.3206598.
[17] P. Li, R. Li, S. Cai, Y. Hong, Intermediate voltage regulation for total harmonic distortion reduction of two-stage inverters under model predictive control scheme via observers, IEEE Access 7 (2019) 51940–51951, http://dx.doi.org/10.1109/ACCESS.2019.2912160.
[18] C. Wang, M. Yang, W. Zheng, J. Long, D. Xu, Vibration suppression with shaft torque limitation using explicit MPC-PI switching control in elastic drive systems, IEEE Trans. Ind. Electron. 62 (11) (2015) 6855–6867, http://dx.doi.org/10.1109/TIE.2015.2438055.
[19] I. Khan, S. Doolla, A PI-MPC based dual-loop controller for grid forming inverters, in: 2023 IEEE International Conference on Environment and Electrical Engineering and 2023 IEEE Industrial and Commercial Power Systems Europe, EEEIC / I&CPS Europe, 2023, pp. 1–6, http://dx.doi.org/10.1109/EEEIC/ICPSEurope57605.2023.10194814.
[20] B. Talbi, F. Krim, A. Laib, A. Sahli, A. Krama, PI-MPC switching control for DC–DC boost converter using an adaptive sliding mode observer, in: 2020 International Conference on Electrical Engineering, ICEE, 2020, pp. 1–5, http://dx.doi.org/10.1109/ICEE49691.2020.9249934.
[21] A. Mironova, B. Haus, A. Zedler, P. Mercorelli, Extended Kalman filter for temperature estimation and control of peltier cells in a novel industrial milling process, IEEE Trans. Ind. Appl. 56 (2) (2020) 1670–1678, http://dx.doi.org/10.1109/TIA.2020.2965058.
[22] A. Walz-Lange, G. Schullerus, Sensorless control of a switched reluctance machine based on switching frequency evaluation, IEEE Trans. Ind. Appl. (2022) 1, http://dx.doi.org/10.1109/TIA.2022.3173595.
[23] P. Mercorelli, A hysteresis hybrid extended Kalman filter as an observer for sensorless valve control in camless internal combustion engines, IEEE Trans. Ind. Appl. 48 (6) (2012) 1940–1949.
[24] P. Mercorelli, A two-stage augmented extended Kalman filter as an observer for sensorless valve control in camless internal combustion engines, IEEE Trans. Ind. Electron. 59 (11) (2012) 4236–4247.
[25] P. Mercorelli, A two-stage sliding-mode high-gain observer to reduce uncertainties and disturbances effects for sensorless control in automotive applications, IEEE Trans. Ind. Electron. 62 (9) (2015) 5929–5940.
[26] K. Scicluna, C.S. Staines, R. Raute, High frequency injection-based sensorless position estimation in permanent magnet synchronous machines, Math. Comput. Simulation 184 (2021) 137–152, http://dx.doi.org/10.1016/j.matcom.2020.02.024.
[27] P. Mercorelli, A motion-sensorless control for intake valves in combustion engines, IEEE Trans. Ind. Electron. 64 (4) (2017) 3402–3412, http://dx.doi.org/10.1109/TIE.2016.2598314.
[28] Y. Yu, X. Huang, Z. Li, M. Wu, T. Shi, Y. Cao, G. Yang, F. Niu, Full parameters estimation for permanent magnet synchronous motors, IEEE Trans. Ind. Electron. (2021) 1, http://dx.doi.org/10.1109/TIE.2021.3078391.
[29] S. Mukundan, H. Dhulipati, J. Tjong, N.C. Kar, Parameter determination of PMSM using coupled electromagnetic and thermal model incorporating current harmonics, IEEE Trans. Magn. 54 (11) (2018) 1–5, http://dx.doi.org/10.1109/TMAG.2018.2837087.
[30] S. Ye, X. Yao, A modified flux sliding-mode observer for the sensorless control of PMSMs with online stator resistance and inductance estimation, IEEE Trans. Power Electron. 35 (8) (2020) 8652–8662, http://dx.doi.org/10.1109/TPEL.2019.2963112.
[31] P. Mercorelli, A two-stage augmented extended Kalman filter as an observer for sensorless valve control in camless internal combustion engines, IEEE Trans. Ind. Electron. 59 (11) (2012) 4236–4247, http://dx.doi.org/10.1109/TIE.2012.2192892.
[32] P. Mercorelli, A hysteresis hybrid extended Kalman filter as an observer for sensorless valve control in camless internal combustion engines, IEEE Trans. Ind. Appl. 48 (6) (2012) 1940–1949, http://dx.doi.org/10.1109/TIA.2012.2226193.
[33] R.E. Kalman, A new approach to linear filtering and prediction problems, J. Basic Eng. 82 (1) (1960) 35–45, http://dx.doi.org/10.1115/1.3662552, arXiv:https://asmedigitalcollection.asme.org/fluidsengineering/article-pdf/82/1/35/5518977/35_1.pdf.
[34] K.E. Myers, B.D. Tapley, Adaptive sequential estimation with unknown noise statistics, IEEE Trans. Autom. Control (1976) 520–523.
[35] K.L. Shi, T.F. Chan, Y.K. Wong, S.L. HO, Speed estimation of an induction motor drive using an optimized extended Kalman filter, IEEE Trans. Ind. Electron. 49 (1) (2002) 124–133.
[36] L. Ortombina, D. Pasqualotto, F. Tinazzi, M. Zigliotto, Automatic tuning procedure at standstill for extended Kalman filter in sensorless control of permanent magnet synchronous motors, in: 10th IEEE International Symposium on Sensorless Control for Electrical Drives, SLED 2019, 2019, pp. 124–133, http://dx.doi.org/10.1109/SLED.2019.8896350.
[37] Q. Song, Y. He, Adaptive unscented Kalman filter for estimation of modelling errors for helicopter, in: 2009 IEEE International Conference on Robotics and Biomimetics, ROBIO, 2009, pp. 2463–2467, http://dx.doi.org/10.1109/ROBIO.2009.5420406.
[38] S. Ritter, Nonlinear State Estimation and Noise Adaptive Kalman Filter Design for Wind Turbines (Ph.D. thesis), Technische Universitaet Darmstadt, 2020.
[39] Q. Juntong, H. Jianda, W. Zhenwei, Rotorcraft UAV actuator failure estimation with KF-based adaptive UKF algorithm, in: 2008 American Control Conference, 2008, pp. 1618–1623, http://dx.doi.org/10.1109/ACC.2008.4586723.
[40] M. Mohamed, I. Kar, Aerodynamic parameter estimation using adaptive unscented Kalman filter, Aircr. Eng. Aerosp. Technol. 85 (2013) http://dx.doi.org/10.1108/AEAT-Mar-2011-0038.
[41] G. Rinaldi, P.P. Menon, C. Edwards, A. Ferrara, Sliding mode based dynamic state estimation for synchronous generators in power systems, IEEE Control Syst. Lett. 2 (4) (2018) 785–790, http://dx.doi.org/10.1109/LCSYS.2018.2849585.
[42] E. Ghahremani, I. Kamwa, Dynamic state estimation in power system by applying the extended Kalman filter with unknown inputs to phasor measurements, IEEE Trans. Power Syst. 26 (4) (2011) 2556–2566, http://dx.doi.org/10.1109/TPWRS.2011.2145396.
[43] S. Bolognani, L. Ortombina, F. Tinazzi, M. Zigliotto, Model sensitivity of fundamental-frequency based position estimators for sensorless PM and reluctance synchronous motor drives, IEEE Trans. Ind. Electron. 65 (1) (2018) http://dx.doi.org/10.1109/TIE.2017.2716902.
[44] M. De Soricellis, D. Da Ru, S. Bolognani, A robust current control based on proportional-integral observers for permanent magnet synchronous machines, IEEE Trans. Ind. Appl. 54 (2) (2018) 1437–1447, http://dx.doi.org/10.1109/TIA.2017.2772171.
[45] S. Bolognani, L. Tubiana, M. Zigliotto, EKF-based sensorless IPM synchronous motor drive for flux-weakening applications, IEEE Trans. Ind. Appl. 39 (3) (2003) 768–775, http://dx.doi.org/10.1109/TIA.2003.810666.
[46] A. Bado, S. Bolognani, M. Zigliotto, Effective estimation of speed and rotor position of a PM synchronous motor drive by a Kalman filtering technique, in: PESC '92 Record. 23rd Annual IEEE Power Electronics Specialists Conference, vol. 2, 1992, pp. 951–957, http://dx.doi.org/10.1109/PESC.1992.254781.
[47] D. Schroeder, Elektrische Antriebe - Grundlagen, Springer Verlag, München, 2016.
[48] T. Zwerger, P. Mercorelli, Backward extended Kalman filter to estimate and adaptively control a PMSM in saturation conditions, IEEE Trans. Emerg. Sel. Topics Power Electron. (2023) 1–14, http://dx.doi.org/10.1109/JESTIE.2023.3313066.
[49] G. Welch, G. Bishop, An Introduction to the Kalman Filter, Prentice Hall, Chapel Hill, NC, USA, Univ. North Caroline Chapel Hill, 1995.
[50] T. Zwerger, P. Mercorelli, A control scheme for PMSMs using model predictive control and a feedforward action in the presence of saturated inputs, in: 2021 22nd International Carpathian Control Conference, ICCC, 2021, pp. 1–6, http://dx.doi.org/10.1109/ICCC51557.2021.9454662.

[51] T. Zwerger, P. Mercorelli, Using a bivariate polynomial in an EKF for state and inductance estimations in the presence of saturation effects to adaptively control a PMSM, IEEE Access 10 (2022) 111545–111553, http://dx.doi.org/10.1109/ACCESS.2022.3215511.
[52] M. Taherzadeh, M.A. Hamida, M. Ghanes, M. Koteich, A new torque observation technique for a PMSM considering unknown magnetic conditions, IEEE Trans. Ind. Electron. 68 (3) (2021) 1961–1971, http://dx.doi.org/10.1109/TIE.2020.2972429.
[53] T. Zwerger, P. Mercorelli, Combining a PI controller with an adaptive feedforward control in PMSM, in: 2020 21th International Carpathian Control Conference, ICCC, 2020, pp. 1–5, http://dx.doi.org/10.1109/ICCC49264.2020.9257288.
[54] G. Basile, G. Marro, Controlled and Conditioned Invariants in Linear System Theory, Prentice Hall, New Jersey-USA, 1992.
[55] S. Huang, K.K. Tan, T.H. Lee, Applied Predictive Control, Springer-Verlag London, Printed in Great Britain, 2002.
[56] P. Mercorelli, A sufficient asymptotic stability condition in generalised model predictive control to avoid input saturation, in: K. Ntalianis, A. Croitoru (Eds.), Applied Physics, System Science and Computers II, Springer International Publishing, Cham, 2019, pp. 251–257.
[57] J. Slotine, W. Li, Applied Nonlinear Control, Prentce-Hall International, Inc., New Jersy, 1991.
[58] T. Duncan, P. Varaiya, On the solutions of a stochastic control system, SIAM J. Control 9 (3) (1971) 354–371, http://dx.doi.org/10.1137/0309026.
[59] A. Lindquist, On feedback control of linear stochastic systems, SIAM J. Control 11 (2) (1973) 323–343, http://dx.doi.org/10.1137/0311025.
[60] T.T. Georgiou, A. Lindquist, The separation principle in stochastic control, redux, IEEE Trans. Autom. Control 58 (10) (2013) 2481–2494, http://dx.doi.org/10.1109/tac.2013.2259207.